



SISALv2: a comprehensive speleothem isotope database with multiple age–depth models

**Laia Comas-Bru¹, Kira Rehfeld², Carla Roesch², Sahar Amirnezhad-Mozhdehi³, Sandy P. Harrison¹,
 Kamolphat Atsawawaranunt¹, Syed Masood Ahmad⁴, Yassine Ait Brahimi^{5,a}, Andy Baker⁶,
 Matthew Bosomworth¹, Sebastian F. M. Breitenbach⁷, Yuval Burstyn⁸, Andrea Columbu⁹,
 Michael Deininger¹⁰, Attila Demény¹¹, Bronwyn Dixon^{1,12}, Jens Fohlmeister¹³, István Gábor Hatvani¹¹,
 Jun Hu¹⁴, Nikita Kaushal¹⁵, Zoltán Kern¹¹, Inga Labuhn¹⁶, Franziska A. Lechleitner¹⁷,
 Andrew Lorrey¹⁸, Belen Martrat¹⁹, Valdir Felipe Novello²⁰, Jessica Oster²¹, Carlos Pérez-Mejías⁵,
 Denis Scholz¹⁰, Nick Scroton²², Nitesh Sinha^{23,24}, Brittany Marie Ward²⁵, Sophie Warken²⁶,
 Haiwei Zhang⁵, and SISAL Working Group members⁺**

¹School of Archaeology, Geography, and Environmental Science, University of Reading, Reading, UK

²Institute of Environmental Physics and Interdisciplinary Center for Scientific Computing,
 Heidelberg University, Heidelberg, Germany

³School of Geography, University College Dublin, Belfield, Dublin 4, Ireland

⁴Department of Geography, Faculty of Natural Sciences, Jamia Millia Islamia, New Delhi, India

⁵Institute of Global Environmental Change, Xi'an Jiaotong University, Xi'an, Shaanxi, China

⁶Connected Waters Initiative Research Centre, UNSW Sydney, Sydney, New South Wales 2052, Australia

⁷Department of Geography and Environmental Sciences, Northumbria University, Newcastle upon Tyne, UK

⁸The Fredy and Nadine Herrmann Institute Earth Sciences, The Hebrew University of Jerusalem,
 The Edmond J. Safra Campus, Jerusalem 9190401, Israel

⁹Department of Biological, Geological and Environmental Sciences (BiGeA), University of Bologna,
 Via Zamboni 67, 40126, Bologna, Italy

¹⁰Institute for Geosciences, Johannes Gutenberg University Mainz,
 J.-J.-Becher-Weg 21, 55128 Mainz, Germany

¹¹Institute for Geological and Geochemical Research, Research Centre for Astronomy and Earth Sciences,
 1112, Budaörsi út 45, Budapest, Hungary

¹²School of Geography, University of Melbourne, Parkville 3010 VIC, Australia

¹³Potsdam Institute for Climate Impact Research PIK, Potsdam, Germany

¹⁴Department of Earth, Environmental and Planetary Sciences, Rice University, Houston, TX 77005, US

¹⁵Asian School of the Environment, Nanyang Technological University, Singapore

¹⁶Institute of Geography, University of Bremen, Celsiusstraße 2, 28359 Bremen, Germany

¹⁷Department of Earth Sciences, University of Oxford, Oxford OX1 3AN, UK

¹⁸National Institute of Water and Atmospheric Research, Auckland, 1010, New Zealand

¹⁹Department of Environmental Chemistry, Spanish Council for Scientific Research (CSIC),
 Institute of Environmental Assessment and Water Research (IDAEA), Barcelona, Spain

²⁰Institute of Geoscience, University of São Paulo, São Paulo, Brazil

²¹Department of Earth and Environmental Sciences, Vanderbilt University, Nashville, TN 37240, USA

²²School of Earth Sciences, University College Dublin, Belfield, Dublin 4, Ireland

²³Center for Climate Physics, Institute for Basic Science, Busan, 46241, Republic of Korea

²⁴Pusan National University, Busan, 46241, Republic of Korea

²⁵Environmental Research Institute, University of Waikato, Hamilton, New Zealand

²⁶Institute of Earth Sciences and Institute of Environmental Physics,
 Heidelberg University, Heidelberg, Germany

^anow at: Department of Environmental Sciences, University of Basel, Basel, Switzerland

✉ A full list of authors appears at the end of the paper.

Correspondence: Laia Comas-Bru (l.comasbru@reading.ac.uk)

Received: 17 February 2020 – Discussion started: 13 March 2020

Revised: 5 August 2020 – Accepted: 30 August 2020 – Published: 27 October 2020

Abstract. Characterizing the temporal uncertainty in palaeoclimate records is crucial for analysing past climate change, correlating climate events between records, assessing climate periodicities, identifying potential triggers and evaluating climate model simulations. The first global compilation of speleothem isotope records by the SISAL (Speleothem Isotope Synthesis and Analysis) working group showed that age model uncertainties are not systematically reported in the published literature, and these are only available for a limited number of records (ca. 15 %, $n = 107/691$). To improve the usefulness of the SISAL database, we have (i) improved the database's spatio-temporal coverage and (ii) created new chronologies using seven different approaches for age–depth modelling. We have applied these alternative chronologies to the records from the first version of the SISAL database (SISALv1) and to new records compiled since the release of SISALv1. This paper documents the necessary changes in the structure of the SISAL database to accommodate the inclusion of the new age models and their uncertainties as well as the expansion of the database to include new records and the quality-control measures applied. This paper also documents the age–depth model approaches used to calculate the new chronologies. The updated version of the SISAL database (SISALv2) contains isotopic data from 691 speleothem records from 294 cave sites and new age–depth models, including age–depth temporal uncertainties for 512 speleothems. SISALv2 is available at <https://doi.org/10.17864/1947.256> (Comas-Bru et al., 2020a).

1 Introduction

Speleothems are a rich terrestrial palaeoclimate archive that forms from infiltrating rainwater after it percolates through the soil, epikarst and carbonate bedrock. In particular, stable oxygen and carbon isotope ($\delta^{18}\text{O}$, $\delta^{13}\text{C}$) measurements made on speleothems have been widely used to reconstruct regional and local hydroclimate changes.

The Speleothem Isotope Synthesis and Analyses (SISAL) working group is an international effort under the auspices of Past Global Changes (PAGES) to compile speleothem isotopic records globally for the analysis of past climates (Comas-Bru and Harrison, 2019). The first version of the SISAL database (Atsawawaranunt et al., 2018a, b) contained 381 speleothem records from 174 cave sites and has been used for analysing regional climate changes (Braun et al., 2019a; Burstyn et al., 2019; Comas-Bru and Harrison, 2019; Deininger et al., 2019; Kaushal et al., 2018; Kern et al., 2019; Lechleitner et al., 2018; Oster et al., 2019; Zhang et al., 2019). The potential for using the SISAL database to evaluate climate models was explored using an updated version of the database (SISALv1b; Atsawawaranunt et al., 2019) that contains 455 speleothem records from 211 sites (Comas-Bru et al., 2019).

SISAL is continuing to expand the global database by including new records (Comas-Bru et al., 2020a). Although most of the records in SISALv2 (79.7 %; Fig. 1a) have been dated using the generally very precise, absolute radiometric $^{230}\text{Th}/\text{U}$ dating method, a variety of age-modelling approaches were employed (Fig. 1b) in constructing the orig-

inal records. The vast majority of records provide no information on the uncertainty of the age–depth relationship. However, many of the regional studies using SISAL pointed to the limited statistical power of analyses of speleothem records because of the lack of temporal uncertainties. For example, these missing uncertainties prevented the extraction of underlying climate modes during the last 2000 years in Europe (Lechleitner et al., 2018). To overcome this limitation, we have developed additional age–depth models for the SISALv2 records (Fig. 2) in order to provide robust chronologies with temporal uncertainties. The results of the various age–depth modelling approaches differ because of differences in their underlying assumptions. We have used seven alternative methods: linear interpolation, linear regression, Bchron (Haslett and Parnell, 2008), Bacon (Blaauw and Christen, 2011; Blaauw et al., 2019), OxCal (Bronk Ramsey, 2008, 2009; Bronk Ramsey and Lee, 2013), COPRA (Brettenbach et al., 2012) and StalAge (Scholz and Hoffmann, 2011). Comparison of these different approaches provides a robust measure of the age uncertainty associated with any specific speleothem record.

2 Data and methods

2.1 Construction of age–depth models: the SISAL chronology

We attempted to construct age–depth models for 533 entities in an automated mode. For eight records, this automated construction failed for all methods. For these records we provide

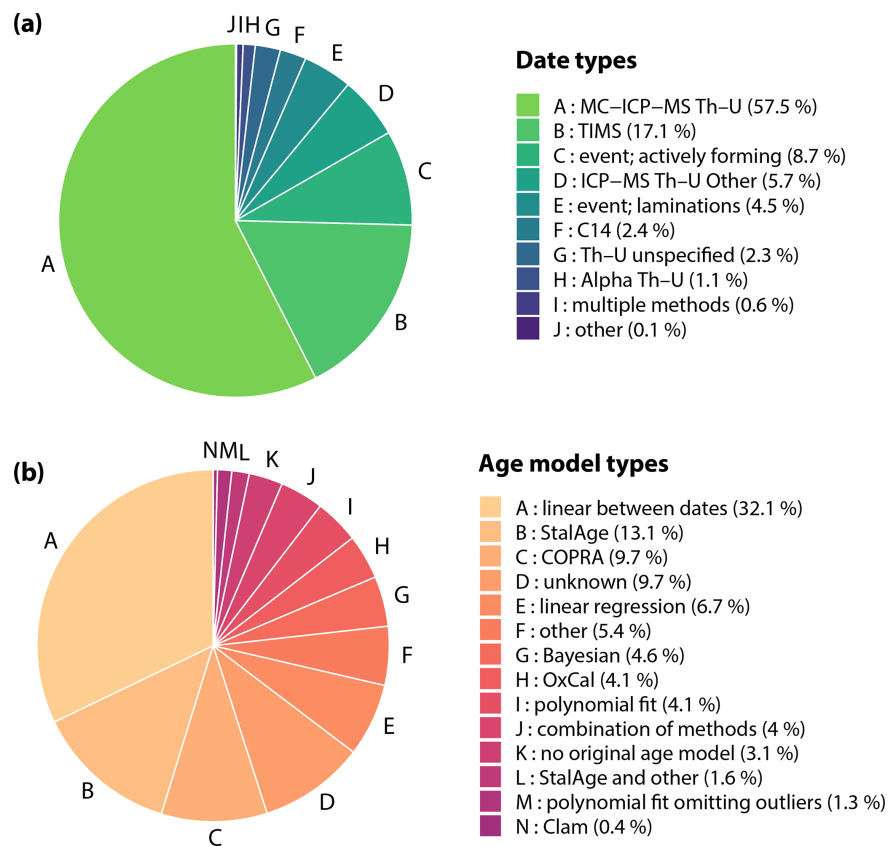


Figure 1. Summary of the dating information on which the original age–depth models are based **(a)** and the original age–depth model types **(b)** present in SISALv2.

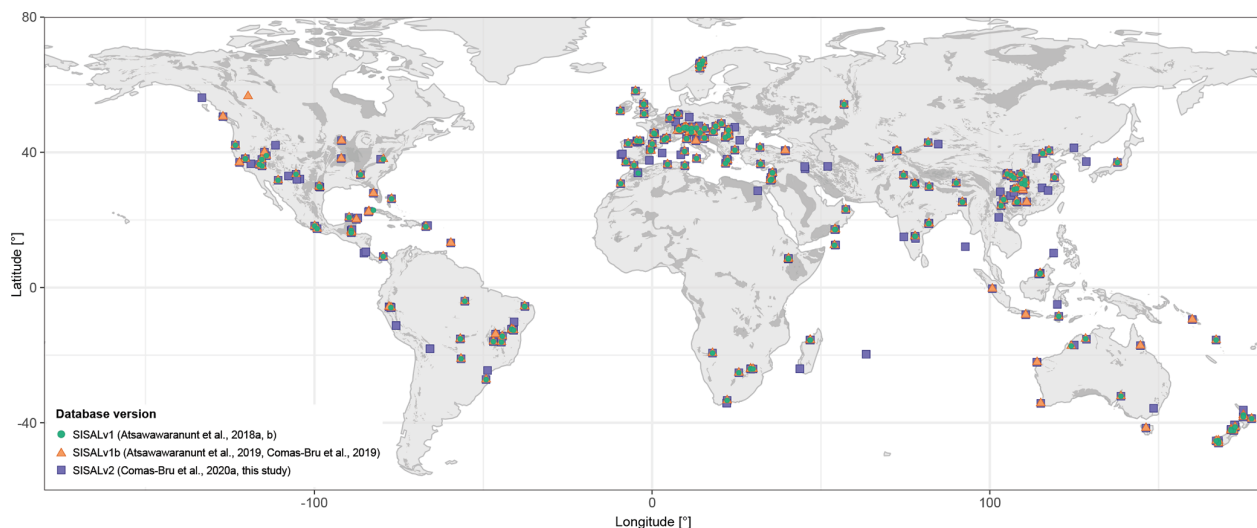


Figure 2. Cave sites included in the version 1, 1b and 2 of the SISAL database on the World Karst Aquifer Map (WOKAM; Goldscheider et al., 2020).

manually constructed chronologies where no age model previously existed and added a note in the database with details on the construction procedure. Age models for 21 records were successfully computed but later dropped in the screening process due to inconsistent information or incompatibility for an automated routine. In total, we provide additional chronologies for 512 speleothem records in SISALv2.

The SISAL chronology provides alternative age–depth models for SISAL records that are not composites (i.e. time series based on more than one speleothem record), that have not been superseded in the database by a newer entity and which are purely $^{230}\text{Th}/\text{U}$ dated. We therefore excluded records for which the chronology is based on lamina counting, radiocarbon ages or a combination of methods. This decision was based on the low uncertainties of the age–depth models based on lamina counting and the challenge of reproducing age–depth models based on radiocarbon ages. We made an exception with the case of entity_id 163 (Talma et al., 1992), which covers two key periods – the mid-Holocene and the Last Glacial Maximum – at high temporal resolution. In this case, we calculated a new SISAL chronology based on the provided $^{230}\text{Th}/\text{U}$ dates but did not consider the uncorrected ^{14}C ages upon which the original age–depth model is based. We also excluded records for which isotopic data are not available (i.e. entities that are part of composites) and entities that are constrained by less than three dates. Additionally, the dating information for 23 entities shows hiatuses at the top and bottom of the speleothem that are not constrained by any date. For these records, we partially masked the new chronologies to remove the unconstrained section(s). Original dates were used without modification in the age–depth modelling.

To allow a comprehensive cross-examination of uncertainties, seven age–depth modelling techniques were implemented here across all selected records. Due to the high number of records ($n = 533$), all methods were run in batch mode. A preliminary study using the database version v1b demonstrated the feasibility of the automated construction and evaluation of age–depth models using a subset of records and methods (Roesch and Rehfeld, 2019). Further details on the evaluation of the updated age–depth models are provided in Sect. 3.2. The seven different methods are briefly described below. All methods assume that growth occurred along a single growth axis. For one entity, where it was previously known that two growth axes exist, we added an explanatory statement in the database. All approaches except StalAge produce Monte Carlo (MC) iterations of the age–depth models. We aimed to provide 1000 MC iterations for each new SISALv2 chronology at <https://doi.org/10.5281/zenodo.3816804> (Rehfeld et al., 2020), but this was not always possible because some records ($n = 12$) yield a substantial number of non-monotonic ensembles that were not kept.

Major challenges arise through hiatuses (growth interruptions) and age reversals. We developed a workflow to deal

with records with known hiatuses that allowed the construction of age–depth models for 20 % of the records with one or more hiatuses (Roesch and Rehfeld, 2019; details below for each age–depth modelling technique). Regarding the age reversals, we distinguish between tractable reversals (with overlapping confidence intervals) and non-tractable reversals (i.e. where the 2-sigma dating uncertainties do not overlap) following the definition of Breitenbach et al. (2012). Details such as the hiatus treatment and outlier age modification are recorded in a log file created when running the age models. We followed the original author's choices regarding date usage. If an age was marked as “not used” or “usage unknown”, we did not consider this in the construction of the new chronologies except in OxCal, where dates with “usage unknown” were considered.

1. Linear interpolation (*lin_interp_age*) between radiometric dates is the classic approach for age–depth model construction for palaeoclimate archives and was used in 32.1 % of the original age–depth models in SISALv2. Here, we extend this approach and calculate the age uncertainty by sampling the range of uncertainty of each $^{230}\text{Th}/\text{U}$ age 2000 times, assuming a Gaussian distribution. This approach is consistent with the implementation of linear interpolation in CLAM (Blaauw, 2010) and COPRA (Breitenbach et al., 2012). Linear interpolation was implemented in R (R Core Team, 2019), using the `approxExtrap()` function in the `Hmisc` package. We included an automated reversal check that increases the dating uncertainties until a monotonic age model is achieved, similar to that of StalAge (Scholz and Hoffmann, 2011). Hiatuses are modelled following the approach of Roesch and Rehfeld (2019), where rather than modelling each segment separately, synthetic ages with uncertainties spanning the entire hiatus duration are introduced for use in age–depth model construction. These synthetic ages are removed after age–depth model construction. Linear interpolation was applied to 80 % ($n = 408/512$) of the SISAL records for which new chronologies were developed.
2. Linear regression (*lin_reg_age*) provides a single best-fit line through all available radiometric ages assuming a constant growth rate. Linear regression was used in 6.7 % of the original SISALv2 age models. As with linear interpolation, age uncertainties are based on randomly sampling the U-series dates to produce 2000 age–depth models (i.e. ensembles). Temporal uncertainties are then given by the uncertainty of the median-based fit to each ensemble member. If hiatuses are present, the segments in-between were split at the depth of the hiatus without an artificial age. The method is implemented in R using the `lm()` function from the base package. Linear regression was applied to 36 % ($n = 185/512$) of the SISAL records for which new chronologies were developed.

3. Bchron (*Bchron_age*) is a Bayesian method based on a continuous Markov processes (Haslett and Parnell, 2008) and is available as an R package (Parnell, 2018). This method was originally used for only one speleothem record in SISALv2. Since Bchron cannot handle hiatuses, we implemented a new workflow that adds synthetic ages with uncertainties spanning the entire hiatus duration (Roesch and Rehfeld, 2019), as performed with linear interpolation, StalAge and our implementation of COPRA. Bchron provides age–depth model ensembles, of which we have kept the last 2000. We calculate the age uncertainties from the spread of the individual ensembles. Here we use the function `bchron()` with `jitter.positions=true` to mitigate problems due to rounded-off depth values. This method has been applied to 83 % ($n = 426/512$) of the SISAL records for which new chronologies were developed.
4. Bacon (*Bacon_age*) is a semi-parametric Bayesian method based on autoregressive gamma processes (Blaauw and Christen, 2011; Blaauw et al., 2019). It was used in three of the original chronologies in SISALv2. The R package *rBacon* can handle both outliers and hiatuses, and apart from giving the median age–depth model, it also returns the Monte Carlo realizations (i.e. ensembles), from which the median age–depth model is calculated. During the creation of the SISAL chronologies, the existing *rBacon* package (version 2.3.9.1) was updated to improve the handling of stalagmite growth rates and hiatuses. We use this revised version, available on CRAN (<https://cran.r-project.org/web/packages/rbacon/index.html>, last access: 31 January 2020), to provide a median age–depth model and an ensemble of age model realizations for 65 % ($n = 335/512$) of the SISAL records for which new chronologies were developed.
5. OxCal (*Oxcal_age*) is a Bayesian chronological modelling tool that uses Markov chain Monte Carlo (Bronk Ramsey, 2009). This method was used in 4.1 % of the original SISALv2 chronologies. OxCal can deal with hiatuses and outliers and accounts for the non-uniform nature of the deposition process (Poisson process using the `P_Sequence` command). Here we used the analysis module of OxCal version 4.3 with a default initial interpolation rate value of 1 and an initial model rigidity (k) value of $k_0 = 1$ with a uniform distribution from 0.01 to 100 for the range of k/k_0 ($\log_{10}(k/k_0) = (-2, 2)$) (Christopher Bronk Ramsey, personal communication, 2019). The initial value of the interpolation rate determines the number of points between any two dates for which an age will be calculated. We subsequently linearly interpolated the age–depth model to the depths of individual isotope measurements. Where multiple dates are given for the same depth for any given entity, the date with the smallest uncertainty was used to construct the SISAL chronology. In the case of asymmetric uncertainties in the dating table, the largest uncertainty value was chosen. We kept the last 2000 realizations of the age–depth models for each entity. We calculate the age uncertainties from the spread of the individual ensembles. Details of the workflow used to construct these chronologies are available in Amirnezhad-Mozhdehi and Comas-Bru (2019). OxCal chronologies are available for 21 % ($n = 106/512$) of the SISAL records for which new chronologies were developed.
6. COPRA (*copRa_age*) is an approach based on interpolation between dates (Breitenbach et al., 2012) and was used for 9.7 % of the original SISALv2 chronologies. COPRA is available as a MATLAB package in Rehfeld et al. (2017) with a graphical user interface (GUI) that has interactive checks for reversals and hiatuses. The MATLAB version can handle multiple hiatuses and (to some extent) layer-counted segments. However, age reversals can occur near short-lived hiatuses. To overcome this, we implemented a new workflow in R that adds artificial dates at the location of the hiatuses and prevents the creation of age reversals (Roesch and Rehfeld, 2019) as done with linear interpolation, StalAge and Bchron. Additionally, we also incorporated an automated reversal check similar to that already embedded into StalAge (Scholz and Hoffmann, 2011). This R version, *copRa*, uses the default piecewise cubic Hermite interpolation (`pchip`) algorithm in R without consideration of layer counting. We calculate the age uncertainties from the spread of the individual ensembles. This approach was used for 76 % ($n = 389/512$) of the SISAL records for which new chronologies were developed.
7. StalAge (*StalAge_age*) fits straight lines through three adjacent dates using weights based on the dating measurement errors (Scholz and Hoffmann, 2011). Age uncertainties are iteratively obtained through a Monte Carlo approach, but ensembles are not given in the output. StalAge was used to construct 13.1 % of the original SISALv2 chronologies. The StalAge v1.0 R function has been updated to R version 3.4, and the default outlier and reversal checks were enabled to run automatically. Hiatuses cannot be entered in StalAge v1.0, but the updated version incorporates a treatment of hiatuses based on the creation of temporary synthetic ages following Roesch and Rehfeld (2019). In contrast to other methods, mean ages instead of median ages are reported for StalAge, and the uncertainties are internally calculated and based on iterative fits considering dating uncertainties. StalAge was applied to 62 % ($n = 320/512$) of the SISAL records for which new chronologies were developed.

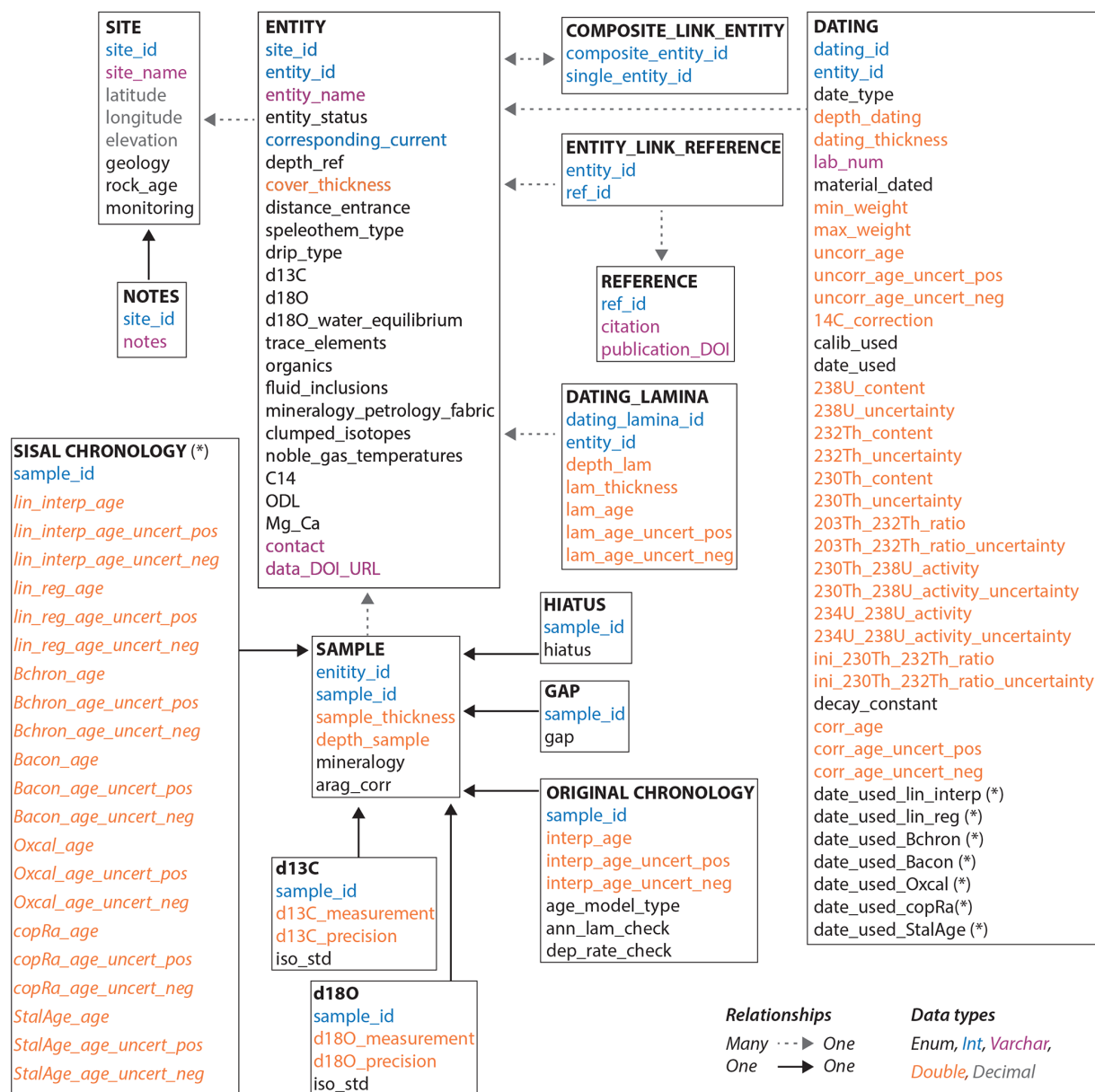


Figure 3. The structure of the SISAL database version 2. Fields and tables marked with (*) refer to new information added to SISALv1b; see Tables 1 and 2 for details. The colours refer to the format of that field: Enum, Int, Varchar, Double or Decimal. More information on the list of predefined menus can be found in Atsawawaranunt et al. (2018a).

2.2 Revised structure of the database

The data are stored in a relational database (MySQL), which consists of 15 linked tables: *site*, *entity*, *sample*, *dating*, *dating_lamina*, *gap*, *hiatus*, *original_chronology*, *d13C*, *d18O*, *entity_link_reference*, *references*, *composite_link_entity*, *notes* and *sisal_chronology*. Figure 3 shows the relationships between these tables and the type of each field (e.g. numeric, text). The structure and contents of all tables except the new *sisal_chronology* table are described in detail in Atsawawaranunt et al. (2018a). Here, we focus on

the new *sisal_chronology* table and on the changes that were made to other tables in order to accommodate this new table (see Sect. 2.3). Details of the fields in this new table are listed in Table 1.

Changes were also made to the dating table (*dating*) to accommodate information about whether a specific date was used to construct each of the age–depth models in the *sisal_chronology* table (Table 2). We followed the original authors’ decision regarding the exclusion of dates (i.e. because of high uncertainties, age reversals or high detrital content). However, some dates used in the orig-

Table 1. Details of the *sisal_chronology* table. All ages in SISAL are reported as years BP (before present), where present is 1950 CE.

Field label	Description	Format	Constraints
<i>sample_id</i>	Refers to the unique identifier for the sample (as given in the sample table)	Numeric	Positive integer
<i>lin_interp_age</i>	Age of the sample in years, calculated with linear interpolation between dates	Numeric	None
<i>lin_interp_age_uncert_pos</i>	Positive 2-sigma uncertainty of the age of the sample in years, calculated with linear interpolation between dates	Numeric	Positive decimal
<i>lin_interp_age_uncert_neg</i>	Negative 2-sigma uncertainty of the age of the sample in years, calculated with linear interpolation between dates	Numeric	Positive decimal
<i>lin_reg_age</i>	Age of the sample in years, calculated with linear regression	Numeric	None
<i>lin_reg_age_uncert_pos</i>	Positive 2-sigma uncertainty of the age of the sample in years, calculated with linear regression	Numeric	Positive decimal
<i>lin_reg_age_uncert_neg</i>	Negative 2-sigma uncertainty of the age of the sample in years, calculated with linear regression	Numeric	Positive decimal
<i>Bchron_age</i>	Age of the sample in years, calculated with Bchron	Numeric	None
<i>Bchron_age_uncert_pos</i>	Positive 2-sigma uncertainty of the age of the sample in years, calculated with Bchron	Numeric	Positive decimal
<i>Bchron_age_uncert_neg</i>	Negative 2-sigma uncertainty of the age of the sample in years, calculated with Bchron	Numeric	Positive decimal
<i>Bacon_age</i>	Age of the sample in years, calculated with Bacon	Numeric	None
<i>Bacon_age_uncert_pos</i>	Positive 2-sigma uncertainty of the age of the sample in years, calculated with Bacon	Numeric	Positive decimal
<i>Bacon_age_uncert_neg</i>	Negative 2-sigma uncertainty of the age of the sample in years, calculated with Bacon	Numeric	Positive decimal
<i>OxCal_age</i>	Age of the sample in years, calculated with OxCal	Numeric	None
<i>OxCal_age_uncert_pos</i>	Positive 2-sigma uncertainty of the age of the sample in years, calculated with OxCal	Numeric	Positive decimal
<i>OxCal_age_uncert_neg</i>	Negative 2-sigma uncertainty of the age of the sample in years, calculated with OxCal	Numeric	Positive decimal
<i>copRa_age</i>	Age of the sample in years, calculated with copRa	Numeric	None
<i>copRa_age_uncert_pos</i>	Positive 2-sigma uncertainty of the age of the sample in years, calculated with copRa	Numeric	Positive decimal
<i>copRa_age_uncert_neg</i>	Negative 2-sigma uncertainty of the age of the sample in years, calculated with copRa	Numeric	Positive decimal
<i>Stalage_age</i>	Age of the sample in years, calculated with StalAge	Numeric	None
<i>Stalage_age_uncert_pos</i>	Positive 2-sigma uncertainty of the age of the sample in years, calculated with StalAge	Numeric	Positive decimal
<i>Stalage_age_uncert_neg</i>	Negative 2-sigma uncertainty of the age of the sample in years, calculated with StalAge	Numeric	Positive decimal

Table 2. Changes made to the dating table to accommodate the new age models. These changes are marked with (*) in Fig. 3.

Action	Field label	Description	Format	Constraints
Field added	<i>date_used_lin_age</i>	Indication whether that date was used to construct the linear age model	Text	Selected from predefined list: “yes”, “no”
Field added	<i>date_used_lin_reg</i>	Indication whether that date was used to construct the age model based on linear regression	Text	Selected from predefined list: “yes”, “no”
Field added	<i>date_used_Bchron</i>	Indication whether that date was used to construct the age model based on Bchron	Text	Selected from predefined list: “yes”, “no”
Field added	<i>date_used_Bacon</i>	Indication whether that date was used to construct the age model based on Bacon	Text	Selected from predefined list: “yes”, “no”
Field added	<i>date_used_OxCal</i>	Indication whether that date was used to construct the age model based on OxCal	Text	Selected from predefined list: “yes”, “no”
Field added	<i>date_used_copRa</i>	Indication whether that date was used to construct the copRa-based age model	Text	Selected from predefined list: “yes”, “no”
Field added	<i>date_used_StalAge</i>	Indication whether that date was used to construct the age model based on StalAge	Text	Selected from predefined list: “yes”, “no”

inal age–depth model were not used in the SISALv2 chronologies to prevent unrealistic age–depth relationships (i.e. age inversions). Information on whether a particular date was used for the construction of specific type of age–depth model is provided in the dating table under columns labelled *date_used_lin_interp*, *date_used_lin_reg*, *date_used_Bchron*, *date_used_Bacon*, *date_used_OxCal*, *date_used_copRa* and *date_used_StalAge* (Table 2).

The dating and the sample tables were modified to accommodate the inclusion of new entities in the database. Specifically, the predefined option lists were expanded, options that had never been used were removed, and some typographical errors in the field names were corrected; these changes are listed in Table 3.

3 Quality control

3.1 Quality control of individual speleothem records

The quality control procedure for individual records newly incorporated in the SISALv2 database is based on the steps described in Atsawawaranunt et al. (2018a). We have updated the Python database scripts to provide a more thorough quality assessment of individual records. Additional checks of the dating table resulted in modifications in the *230Th_232Th*, *230Th_238U*, *234U_238U*, *ini230Th_232Th*, *238U_content*, *230Th_content*, *232Th_content* and *decay constant* fields in the dating table for 60 entities. A summary of the fields that

are both automatically and manually checked before uploading a record to the database is available in the Supplement.

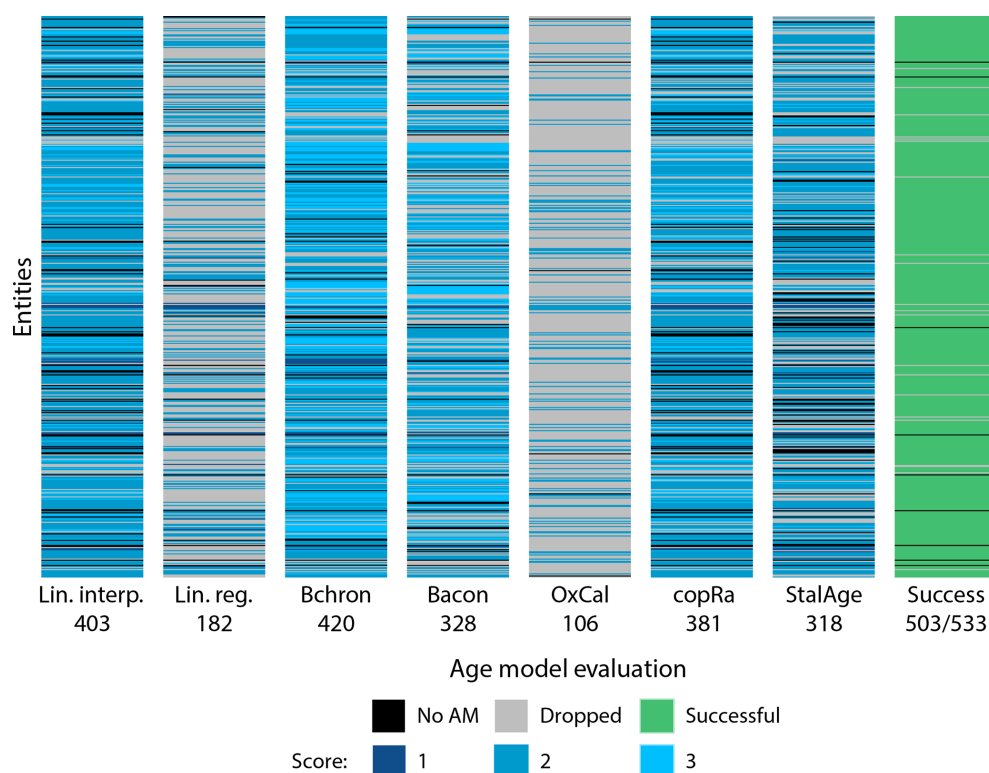
Analyses of the data included in SISALv1 (Braun et al., 2019a; Burstyn et al., 2019; Deininger et al., 2019; Kaushal et al., 2018; Kern et al., 2019; Lechleitner et al., 2018; Oster et al., 2019; Zhang et al., 2019) and SISALv1b (Comas-Bru et al., 2019) revealed a number of errors in specific records that have now been corrected. These revisions include, for example, updates in mineralogies (*sample.mineralogy*), revised coordinates (*site.latitude* and/or *site.longitude*) and addition of missing information that was previously entered as “unknown”. The fields affected and the number of records with modifications are listed in Table 4. All revisions are also documented in Comas-Bru et al. (2020a).

3.2 Automation and quality control of the age–depth models in the SISAL chronology

We used an automated approach to age–depth modelling in R because of the large number of records. Roesch and Rehfeld (2019) have described the basic workflow concept and tested it using all of the age-modelling approaches used here except OxCal. The basic workflow involves step-by-step inspection and formatting of the data for the different methods, and the use of predefined parameter choices is specific to each method. Each age-modelling method is called sequentially. An error message is recorded in the log file if a particular age-modelling method fails, and the algorithm then progresses to the next method. If output is produced for a par-

Table 3. Changes made to tables other than the *sisal_chronology* since the publication of SISALv1 (Atsawawaranunt et al., 2018a, b).

Table name	Action	Field label	Reason	Format	Constraints
Dating	Removed “sampling gap” option	<i>date_type</i>	Option never used	Text	Selected from pre-defined list
	The “others” option changed to “other”	<i>decay_constant</i>	Correction of typo	Text	Selected from pre-defined list
	Added “other” option	<i>calib_used</i>	Option added to accommodate new entities	Text	Selected from pre-defined list
	Added “other” option	<i>date_type</i>	Option added to accommodate new entities	Text	Selected from pre-defined list
Sample	Added “other” option	<i>original_chronology</i>	Option added to accommodate new entities	Text	Selected from pre-defined list
	Added “other” option	<i>ann_lam_check</i>	Option added to accommodate new entities	Text	Selected from pre-defined list

**Figure 4.** Visual summary of quality control of the automated SISAL chronology construction. The evaluation of the age–depth models for each method (*x* axis) is given for each entity (*y* axis) that was considered for the construction ($n = 533$). Black lines mark age–depth models that could not be computed. Age–depth models dropped in the automated or expert evaluation are marked by grey lines. Age–depth models retained in SISALv2 are scored from 1 (only one criterion satisfied) to 3 (all criteria satisfied) in shades of blue. For 503 records alternative age–depth models with uncertainties are provided (green lines) in the “success” column.

ticular age-modelling method, these age models are checked for monotonicity. Finally, the output standardization routine writes out, for each entity and age-modelling approach, the median age model, the ensembles (if applicable) and information of which hiatuses and dates were used in the construction of the age models. These outputs are then added to the *sisal_chronology* table (Table 2). All functions are avail-

able at <https://github.com/paleovar/SISAL.AM> (last access: 23 July 2020).

The general approach for the OxCal age models was similar, and step-by-step details and scripts are provided at <https://doi.org/10.5281/zenodo.3586280> (Amirnezhad-Mozhdehi and Comas-Bru, 2019). The quality control parameters obtained from OxCal were compared with the rec-

Table 4. Summary of the modifications applied to records already in version 1 (Atsawawaranunt et al., 2018b) and version 1b (Atsawawaranunt et al., 2019) of the SISAL database. Mistakes in previous versions of the database were identified as outlined in the Supplement and through analysing the data for the SISAL publications.

Modification	V1 to v1b	V1b to v2
Site table		
Number of new sites	37	82
Sites with new entities	11	32
Sites with altered site.site_name altered	3	15
Sites with changes in site.latitude	4	29
Sites with changes in site.longitude	6	32
Sites with changes in site.elevation	13	11
Sites with site.geology updated	7	6
Sites with site.rock_age info updated	3	8
Sites with site.monitoring info updated	0	13
Entity table		
Number of new entities	74	236
How many entities were added to pre-existing sites?	17	84
Entities with revised entity_name	2	25
Entities with updated entity.entity_status	1	10
Entities with altered entity.corresponding current	0	11
Entities with altered entity.depth_ref?	0	1
Entities with altered entity.cover_thickness	1	3
Entities with altered entity.distance_entrance	0	3
Entities with revised entity. speleothem_type	14	4
Entities with revised entity.drip_type	10	2
Entities with altered entity.d13C	1	0
Entities with altered entity.d18O	1	0
Entities with altered entity.d18O_water_equilibrium	4	6
Entities with altered entity.trace_elements	1	2
Entities with altered entity.organics	1	2
Entities with altered entity.fluid_inclusions	1	3
Entities with altered entity.mineralogy_petrology_fabric	1	2
Entities with altered entity.clumped_isotopes	1	3
Entities with altered entity.noble_gas_temperatures	1	2
Entities with altered entity.C14	1	2
Entities with altered entity.ODL	1	2
Entities with altered entity.Mg_Ca	1	2
Entities with altered entity.contact (mostly correction of typos)	7	32
Entities with altered entity.Data_DOI_URL (revision mostly to permanent links)	134	14
Dating table		
Entities with changes in the dating table	70	269
Addition of “Event: hiatus” to an entity	0	3
How many hiatuses had their depth changed?	2	7
Entities with the depths of “Event: start/end of laminations” changed	0	5
Entities with altered dating.date_type	11	30
Entities with altered dating.depth_dating	14	45
Entities with altered dating.dating_thickness	14	37
Entities with altered dating.material_dated	5	62
Entities with altered dating.min_weight	13	56
Entities with altered dating.max_weight	19	36
Entities with altered dating.uncorr_age	18	48
Entities with altered dating.uncorr_age_uncert_pos	12	53
Entities with altered dating.uncorr_age_uncert_neg	12	40
Entities with altered dating.14C_correction	17	36

Table 4. Continued.

Modification	V1 to v1b	V1b to v2
Entities with altered dating.calib_used	13	32
Entities with altered dating.date_used	4	51
Entities with altered dating.238U_content	11	47
Entities with altered dating.238U_uncertainty	16	29
Entities with altered dating.232Th_content	15	46
Entities with altered dating.232Th_uncertainty	14	50
Entities with altered dating.230Th_content	11	40
Entities with altered dating.230Th_uncertainty	15	38
Entities with altered dating.230Th_232Th_ratio	5	60
Entities with altered dating.230Th_232Th_ratio_uncertainty	14	49
Entities with altered dating.230Th_238U_activity	19	40
Entities with altered dating.230Th_238U_activity_uncertainty	17	49
Entities with altered dating.234U_238U_activity	12	40
Entities with altered dating.234U_238U_activity_uncertainty	11	40
Entities with altered dating.ini_230Th_232Th_ratio	15	41
Entities with altered dating.ini_230Th_232Th_ratio_uncertainty	8	49
Entities with altered dating.decay_constant	17	55
Entities with altered dating.corr_age	17	36
Entities with altered dating.corr_age_uncert_pos	13	47
Entities with altered dating.corr_age_uncert_neg	9	52
Sample table		
Altered sample.depth_sample	0	15
Altered sample.mineralogy	0	20
Altered sample.arag_corr	11	20
How many entities had their d18O time series altered (i.e. changes in depth and/or isotope values as in duplicates)?	13	96
How many entities had their d13C time series altered (i.e. changes in depth and/or isotope values as in duplicates)?	8	64
Original chronology		
Entities with altered original_chronology.interp_age	1	42
Entities with altered original_chronology.interp_age_uncert_pos	0	14
Entities with altered original_chronology.interp_age_uncert_neg	0	14
References		
How many entities had their references changed (changes/additions/removals)?	6	16
How many citations have a different pub_DOI?	2	16
Notes		
Sites with notes removed	7	5
Sites with notes added	32	68
Sites with notes modified	21	33

ommended values of the agreement index (A) > 60 % and convergence (C) > 95 % in accordance with the guidelines in Bronk Ramsey (2008), both for the overall model and for at least 90 % of the individual dates. OxCal age–depth models failing to meet these criteria were not included in the *sisal_chronology* table (Table 2).

An overview of the evaluation results for the age–depth models constructed in automated mode is given in Fig. 4. Three nested criteria are used to evaluate them. Firstly,

chronologies with reversals (Check 1) are automatically rejected (score –1). Secondly, the final chronology should flexibly follow clear growth rate changes (Check 2) such that 70 % of the dates are encompassed in the final age–depth model within 4-sigma uncertainty (score +1). Thirdly, temporal uncertainties are expected to increase between dates and near hiatuses (Check 3). This criterion is met in the automated screening (score +1) if the interquartile range (IQR) is higher between dates or at hiatuses than at dates. Only

Table 5. Information on new speleothem records (entities) added to the SISAL_v2 database from SISALv1b (Comas-Bru et al., 2019). There may be multiple entities from a single cave, here identified as the site. Latitude (Lat) and Longitude (Long) are given in decimal degrees north and east, respectively.

Site ID	Site name	Lat (N)	Long (E)	Region	Entity ID	Entity name	Reference
2	Kesang cave	42.87	81.75	China	620	CNKS-2	Cai et al. (2017)
					621	CNKS-3	Cai et al. (2017)
					622	CNKS-7	Cai et al. (2017)
					623	CNKS-9	Cai et al. (2017)
6	Hulu cave	32.5	119.17	China	617	MSP	Cheng et al. (2006)
					618	MSX	Cheng et al. (2006)
					619	MSH	Cheng et al. (2006)
12	Mawmluh cave	25.2622	91.8817	India	476	ML.1	Kathayat et al. (2018)
					477	ML.2	Kathayat et al. (2018)
					495	KM-1	Huguet et al. (2018)
13	Ball Gown cave	−17.03	125	Australia	633	BGC-5	Denniston et al. (2013b, 2017)
					634	BGC-10	Denniston et al. (2013b, 2017)
					635	BGC-11_2017	Denniston et al. (2013b, 2017)
					636	BGC-16	Denniston et al. (2013b, 2017)
14	Lehman caves	39.01	−114.22	United States	641	CDR3	Steponaitis et al. (2015)
					642	WR11	Steponaitis et al. (2015)
15	Baschg cave	47.2501	9.6667	Austria	643	BA-5	Moseley et al. (2020)
					644	BA-7	Moseley et al. (2020)
23	Lapa grande cave	−14.37	−44.28	Brazil	614	LG12B	Strikis et al. (2018)
					615	LG10	Strikis et al. (2018)
					616	LG25	Strikis et al. (2018)
24	Lapa sem fim cave	−16.1503	−44.6281	Brazil	603	LSF15	Strikis et al. (2018)
					604	LSF3_2018	Strikis et al. (2018)
					605	LSF13	Strikis et al. (2018)
					606	LSF11	Strikis et al. (2018)
					607	LSF9	Strikis et al. (2018)
27	Tamboril cave	−16	−47	Brazil	594	TM6	Ward et al. (2019)
39	Dongge cave	25.2833	108.0833	China	475	DA_2009	Cheng et al. (2009)
54	Sahiya cave	30.6	77.8667	India	478	SAH-2	Kathayat et al. (2017)
					479	SAH-3	Kathayat et al. (2017)
					480	SAH-6	Kathayat et al. (2017)
65	Whiterock cave	4.15	114.86	Malaysia (Borneo)	685	WR12-01	Carolin et al. (2016)
					686	WR12-12	Carolin et al. (2016)
72	Ascunsa cave	45	22.6	Romania	582	POM1	Staubwasser et al. (2018)
82	Hollywood cave	−41.95	171.47	New Zealand	673	HW-1	Williams et al. (2005)
86	Modric cave	44.2568	15.5372	Croatia	631	MOD-27	Rudzka-Phillips et al. (2013)
					632	MOD-21	Rudzka et al. (2012)
105	Schneckenloch cave	47.4333	9.8667	Austria	663	SCH-6	Moseley et al. (2020)
113	Paixao cave	−12.6182	−41.0184	Brazil	611	PX5	Strikis et al. (2015)
					612	PX7_2018	Strikis et al. (2018)
115	Hölloch im Mahdtal	47.3781	10.1506	Germany	664	HOL-19	Moseley et al. (2020)
117	Bunker cave	51.3675	7.6647	Germany	596	Bu2_2018	Weber et al. (2018)
128	Buckeye creek	37.98	−80.4	United States	681	BCC-9	Cheng et al. (2019)
					682	BCC-10_2019	Cheng et al. (2019)
					683	BCC-30	Cheng et al. (2019)
135	Grotte de Piste	33.95	−4.246	Morocco	464	GP5	Ait Brahim et al. (2018)
					591	GP2	Ait Brahim et al. (2018)
138	Moomi cave	12.55	54.2	Yemen (Socotra)	481	M1-2	Mangini, Cheng et al. (unpublished data); Burns et al. (2003, 2004)

Table 5. Continued.

Site ID	Site name	Lat (N)	Long (E)	Region	Entity ID	Entity name	Reference
140	Sanbao cave	31.667	110.4333	China	482	SB3	Wang et al. (2008)
					483	SB-10_2008	Wang et al. (2008)
					484	SB11	Wang et al. (2008)
					485	SB22	Wang et al. (2008)
					486	SB23	Wang et al. (2008)
					487	SB24	Wang et al. (2008)
					488	SB25-1	Wang et al. (2008)
					489	SB25-2	Wang et al. (2008)
					490	SB-26_2008	Wang et al. (2008)
					491	SB34	Wang et al. (2008)
					492	SB41	Wang et al. (2008)
					493	SB42	Wang et al. (2008)
					494	TF	Wang et al. (2008)
141	Sofular cave	41.4167	31.9333	Turkey	456	SO-2	Badertscher et al. (2011) Fleitmann et al. (2009); Göktürk et al. (2011)
					687	SO-4	Badertscher et al. (2011)
					688	SO-6	Badertscher et al. (2011)
					689	SO-14B	Badertscher et al. (2011)
145	Antro del Corchia	43.9833	10.2167	Italy	665	CC-1_2018	Tzedakis et al. (2018)
					666	CC-5_2018	Tzedakis et al. (2018)
					667	CC-7_2018	Tzedakis et al. (2018)
					668	CC-28_2018	Tzedakis et al. (2018)
					669	CC_stack	Tzedakis et al. (2018)
					670	CC27	Isola et al. (2019)
155	KNI-51	−15.3	128.62	Australia	637	KNI-51-1	Denniston et al. (2017)
					638	KNI-51-8	Denniston et al. (2017)
160	Soreq cave	31.7558	35.0226	Israel	690	Soreq-composite185	Bar-Matthews et al. (2003)
165	Ruakuri cave	−36.27	175.08	New Zealand	674	RK-A	Williams et al. (2010)
					675	RK-B	Williams et al. (2010)
					676	RK05-1	Whittaker (2008)
					677	RK05-3	Whittaker (2008)
					678	RK05-4	Whittaker (2008)
177	Santo Tomas cave	22.55	−83.84	Cuba	608	CM_2019	Warken et al. (2019)
					609	CMa	Warken et al. (2019)
					610	CMb	Warken et al. (2019)
179	Closani cave	45.10	22.8	Romania	390	C09-2	Warken et al. (2018)
182	Kotumsar cave	19	82	India	590	KOT-I	Band et al. (2018)
192	El Condor cave	−5.93	−77.3	Peru	592	ELC-A	Cheng et al. (2013)
					593	ELC-B	Cheng et al. (2013)
198	Lianhua cave, Hunan	29.48	109.5333	China	496	LH-2	Zhang et al. (2013)
213	Tausoare cave	47.4333	24.5167	Romania	457	1152	Staubwasser et al. (2018)
214	Cave C126	−22.1	113.9	Australia	458	C126-117	Denniston et al. (2013a)
					459	C126-118	Denniston et al. (2013a)
215	Chaara cave	33.9558	−4.2461	Morocco	460	Cha2_2018	Ait Brahimi et al. (2018)
					588	Cha2_2019	Ait Brahimi et al. (2019)
					589	Cha1	Ait Brahimi et al. (2019)
216	Dark cave	27.2	106.1667	China	461	D1	Jiang et al. (2013)
					462	D2	Jiang et al. (2013)
217	E'mei cave	29.5	115.5	China	463	EM1	Zhang et al. (2018b)
218	Nuanhe cave	41.3333	124.9167	China	465	NH6	Wu et al. (2012)
					466	NH33	Wu et al. (2012)

Table 5. Continued.

Site ID	Site name	Lat (N)	Long (E)	Region	Entity ID	Entity name	Reference
219	Shennong cave	28.71	117.26	China	467	SN17	Zhang et al. (2018a)
220	Baeg-nyong cave	37.27	128.58	South Korea	468	BN-1	Jo et al. (2017)
221	La Vierge cave	−19.7572	63.3703	Rodrigues	469	LAVI-4	Li et al. (2018)
222	Patate cave	−19.7583	63.3864	Rodrigues	470	PATA-1	Li et al. (2018)
223	Wanxiang cave	33.32	105	China	471	WX42B	Zhang et al. (2008)
					679	WXSM-51	Johnson et al. (2006)
					680	WXSM-52	Johnson et al. (2006)
224	Xianglong cave	33	106.33	China	472	XL16	Tan et al. (2018a)
					473	XL2	Tan et al. (2018a)
					474	XL26	Tan et al. (2018a)
225	Chiflonkhakha cave	−18.1222	−65.7739	Bolivia	497	Boto 1	Apaestegui et al. (2018)
					498	Boto 3	Apaestegui et al. (2018)
					499	Boto 7	Apaestegui et al. (2018)
226	Cueva del Diamante	−5.73	−77.5	Peru	500	NAR-C	Cheng et al. (2013)
					501	NAR-C-D	Cheng et al. (2013)
					502	NAR-C-F	Cheng et al. (2013)
					503	NAR-D	Cheng et al. (2013)
					504	NAR-F	Cheng et al. (2013)
227	El Capitan cave	56.162	−133.319	United States	505	EC-16-5-F	Wilcox et al. (2019)
228	Bat cave	32.1	−104.26	United States	506	BC-11	Asmerom et al. (2013)
229	Actun Tunichil Muknal	17.1	−88.85	Belize	507	ATM-7	Frappier et al. (2002, 2007); Jamieson et al. (2015)
230	Marota cave	−12.6227	−41.0216	Brazil	508	MAG	Strfakis et al. (2018)
231	Pacupahuain cave	−11.24	−75.82	Peru	509	P09PH2	Kanner et al. (2012)
232	Rio Secreto cave system	20.59	−87.13	Mexico	510	Itzamna	Medina-Elizalde et al., (2016, 2017)
233	Robinson cave	33	−107.7	United States	511	KR1	Polyak et al. (2017)
234	Santana cave	−24.5308	−48.7267	Brazil	512	St8-a	Cruz et al. (2006)
					513	St8-b	Cruz et al. (2006)
235	Cueva del Tigre Perdido	−5.9406	−77.3081	Peru	514	NC-A	van Breukelen et al. (2008)
					515	NC-B	van Breukelen et al. (2008)
236	Toca da Boa Vista	−10.1602	−40.8605	Brazil	516	TBV40	Wendt et al. (2019)
					517	TBV63	Wendt et al. (2019)
237	Umajalanta cave	−18.12	−65.77	Bolivia	518	Boto 10	Apaestegui et al. (2018)
238	Akalagavi cave	14.9833	74.5167	India	519	MGY	Yadava et al. (2004)
239	Baluk cave	42.433	84.733	China	520	BLK12B	Liu et al. (2019)
240	Baratang cave	12.0833	92.75	India	521	AN4	Laskar et al. (2013)
					522	AN8	Laskar et al. (2013)
241	Gempa bumi cave	−5	120	Indonesia (Sulawesi)	523	GB09-03	Krause et al. (2019)
					524	GB11-09	Krause et al. (2019)
242	Haozhu cave	30.6833	109.9833	China	525	HZZ-11	Zhang et al. (2016)
					526	HZZ-27	Zhang et al. (2016)
243	Kailash cave	18.8445	81.9915	India	527	KG-6	Gautam et al. (2019)
244	Lianhua cave, Shanxi	38.1667	113.7167	China	528	LH1	Dong et al. (2018)
					529	LH4	Dong et al. (2018)
					530	LH5	Dong et al. (2018)
					531	LH6	Dong et al. (2018)
					532	LH9	Dong et al. (2018)
					533	LH30	Dong et al. (2018)

Table 5. Continued.

Site ID	Site name	Lat (N)	Long (E)	Region	Entity ID	Entity name	Reference
245	Nakarallu cave	14.52	77.99	India	534	NK-1305	Sinha et al. (2018)
246	Palawan cave	10.2	118.9	Malaysia (northern Borneo)	535	SR02	Partin et al. (2015)
247	Shalail cave	35.1469	45.2958	Iraq	536	SHC-01	Marsh et al. (2018); Amin Al-Manmi et al. (2019)
					537	SHC-02	Marsh et al. (2018); Amin Al-Manmi et al. (2019)
248	Shenqi cave	28.333	103.1	China	538	SQ1	Tan et al. (2018b)
					539	SQ7	Tan et al. (2018b)
249	Shigao cave	28.183	107.167	China	540	SG1	Jiang et al. (2012)
					541	SG2	Jiang et al. (2012)
250	Wuya cave	33.82	105.43	China	542	WY27	Tan et al. (2015)
					543	WY33	Tan et al. (2015)
251	Zhenzhu cave	38.25	113.7	China	544	ZZ12	Yin et al. (2017)
252	Andriamaniloke	−24.051	43.7569	Madagascar	545	AD4	Scroton et al. (2019)
253	Hoq cave	12.5866	54.3543	Yemen (Socotra)	546	Hq-1	Van Rempelbergh et al. (2013)
					547	STM1	Van Rempelbergh et al. (2013)
					548	STM6	Van Rempelbergh et al. (2013)
254	PP29	−34.2078	22.0876	South Africa	549	46745	Braun et al. (2019b)
					550	46746-a	Braun et al. (2019b)
					551	46747	Braun et al. (2019b)
					552	138862.1	Braun et al. (2019b)
					553	138862.2a	Braun et al. (2019b)
					554	142828	Braun et al. (2019b)
					555	46746-b	Braun et al. (2019b)
					556	138862.2b	Braun et al. (2019b)
255	Mitoho	−24.0477	43.7533	Madagascar	557	MT1	Scroton et al. (2019)
256	Lithophagus cave	46.828	22.6	Romania	558	LFG-2	Lauritzen and Onac (1999)
257	Akcakale cave	40.4498	39.5365	Turkey	559	2p	Jex et al. (2010, 2011, 2013)
258	B7 cave	49	7	Germany	560	STAL-B7-7	Niggemann et al. (2003b)
259	Cobre cave	42.98	−4.37	Spain	561	PA-8	Osete et al. (2012); Rossi et al. (2014)
260	Crovassa Azzurra	39.28	8.48	Italy	562	CA	Columbu et al. (2019)
261	El Soplaio cave	43.2962	−4.3937	Spain	563	SIR-1	Rossi et al. (2018)
262	Bleßberg cave	50.4244	11.0203	Germany	564	BB-1	Breitenbach et al. (2019)
					565	BB-3	Breitenbach et al. (2019)
263	Orlova Chuka cave	43.5937	25.9597	Bulgaria	566	ocz-6	Pawlak et al. (2019)
264	Strašna peć cave	44.0049	15.0388	Croatia	567	SPD-1	Lončar et al. (2019)
					568	SPD-2	Lončar et al. (2019)
265	Coves de Campanet	39.7937	2.9683	Spain	569	CAM-1	Dumitru et al. (2018)
266	Cueva Victoria	37.6322	−0.8215	Spain	570	Vic-III-4	Budsky et al. (2019)
267	Gruta do Casal da Lebre	39.3	−9.2667	Portugal	571	GCL6	Denniston et al. (2018)
268	Pere Noel cave	50	5.2	Belgium	572	PN-95-5	Verheyden et al. (2000, 2014)
269	Gejkar cave	35.8	45.1645	Iraq	573	Gej-1	Flohr et al. (2017)
270	Gol-E-Zard cave	35.84	52	Iran	574	GZ14-1	Carolin et al. (2019)
271	Jersey cave	−35.72	148.49	Australia	575	YB-F1	Webb et al. (2014)
272	Metro cave	−41.93	171.47	New Zealand	576	M-1	Logan (2011)
273	Crystal cave	36.59	−118.82	United States	577	CRC-3	McCabe-Glynn et al. (2013)

Table 5. Continued.

Site ID	Site name	Lat (N)	Long (E)	Region	Entity ID	Entity name	Reference
274	Terciopelo cave	10.17	−85.33	Costa Rica	578	CT-1	Lachniet et al. (2009)
					579	CT-5	Lachniet et al. (2009)
					580	CT-6	Lachniet et al. (2009)
					581	CT-7	Lachniet et al. (2009)
275	Buraca Gloriosa	39.5333	−8.7833	Portugal	583	BG41	Denniston et al. (2018)
					584	BG66	Denniston et al. (2018)
					585	BG67	Denniston et al. (2018)
					586	BG611	Denniston et al. (2018)
					587	BG6LR	Denniston et al. (2018)
276	Béke cave	48.4833	20.5167	Hungary	595	BNT-2	Demény et al. (2019) Czuppon et al. (2018)
277	Huagapo cave	−11.27	−75.79	Peru	597	P00-H2	Kanner et al. (2013)
					598	P00-H1	Kanner et al. (2013)
					599	P09-H1b	Burns et al. (2019)
					600	P10-H5	Burns et al. (2019)
					601	P10-H2	Burns et al. (2019)
					602	PeruMIS6Composite	Burns et al. (2019)
278	Pink Panther cave	32	−105.2	United States	613	PP1	Asmerom et al. (2007)
279	Staircase cave	−34.2071	22.0899	South Africa	624	46322	Braun et al. (2019b)
					625	46330-a	Braun et al. (2019b)
					626	46861	Braun et al. (2019b)
					627	50100	Braun et al. (2019b)
					628	142819	Braun et al. (2019b)
					629	142820	Braun et al. (2019b)
					630	46330-b	Braun et al. (2019b)
280	Atta cave	51.1	7.9	Germany	639	AH-1	Niggemann et al. (2003a)
281	Venado cave	10.55	−84.77	Costa Rica	640	V1	Lachniet et al. (2004)
282	Wadi Sannur cave	28.6167	31.2833	Egypt	691	WS-5d	El-Shenawy et al. (2018)
283	Babylon cave	−41.95	171.47	New Zealand	645	BN-1	Williams et al. (2005)
					646	BN-2	Williams et al. (2005)
					647	BN-3	Lorrey et al. (2010)
284	Creighton's cave	−40.63	172.47	New Zealand	648	CN-1	Williams et al. (2005)
285	Disbelief cave	−38.82	177.52	New Zealand	649	Disbelief	Lorrey et al. (2008)
286	La Garma cave	43.4306	−3.6658	Spain	650	GAR-01_drill	Baldini et al. (2015, 2019)
					651	GAR-01_laser_d18O	Baldini et al. (2015)
					652	GAR-01_laser_d13C	Baldini et al. (2015)
287	Twin Forks cave	−40.63	172.48	New Zealand	653	TF-2	Williams et al. (2005)
288	Wet Neck cave	−40.7	172.48	New Zealand	654	WN-4	Williams et al. (2005)
					655	WN-11	Williams et al. (2005)
289	Gassel Tropfsteinhöhle	47.8228	13.8428	Austria	656	GAS-12	Moseley et al. (2020)
					657	GAS-13	Moseley et al. (2020)
					658	GAS-22	Moseley et al. (2020)
					659	GAS-25	Moseley et al. (2020)
					660	GAS-27	Moseley et al. (2020)
					661	GAS-29	Moseley et al. (2020)
290	Grete-Ruth Shaft	47.5429	12.0272	Austria	662	HUN-14	Moseley et al. (2020)
292	Limnon cave	37.9605	22.1403	Greece	671	KTR-2	Peckover et al. (2019)
293	Tham Doun Mai	20.75	102.65	Laos	672	TM-17	Wang et al. (2019)
294	Palco cave	18.35	−66.5	Puerto Rico	684	PA-2b	Rivera-Collazo et al. (2015)

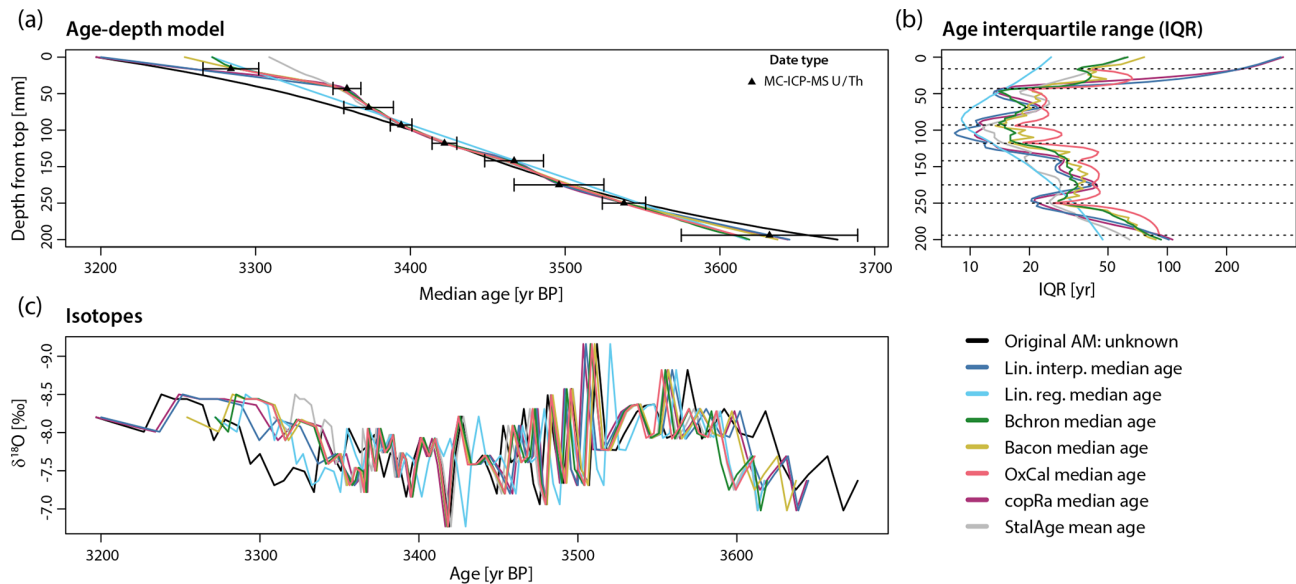


Figure 5. Illustration of the impact of the age model choice on reconstructed speleothem chronology illustrated by the KNI-51-H speleothem record (entity_id 342; Denniston et al., 2013b). Panel (a) shows the median and mean age estimates for each downcore sample from the different age models; (b) shows the interquartile range (IQR) of the ages. Dashed horizontal lines show the depths of the measured dates; (c) shows the isotopic record using the different age models.

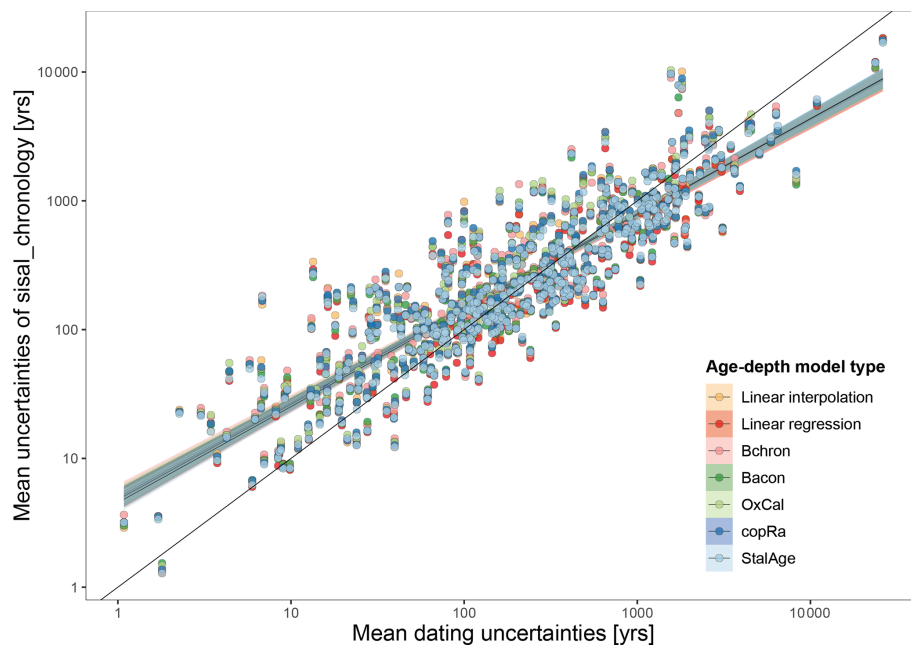


Figure 6. Scatterplot of average uncertainties in the *sisal_chronology* table and ²³⁰Th/U mean dating uncertainties for each entity and age–depth model technique. The 1 : 1 line is shown in black.

entities that pass all three criteria are considered successful. All age–depth models that satisfied Check 1 were also evaluated in an expert-based manual screening by 10 people. If more than two experts agreed that an individual age–depth model was unreliable or inconsistencies, such as large offsets between the original age model and the dates marked as

“used”, occurred, the model was not included in the SISAL chronology table. This automatic and expert-based quality control screening resulted in 2138 new age–depth models constructed for 503 SISAL entities.

4 Recommendation for the use of SISAL chronologies

The original age–depth models for every entity are available in SISALv2. However, given the lack of age uncertainties for most of the records, we recommend considering the SISAL chronologies with their respective 95 % confidence intervals whenever possible. No single age–depth modelling approach is successful for all entities, and we therefore recommend that all the methods for a specific entity are used together in visual and/or statistical comparisons. Depending on methodological choices, age–depth models compatible with the dating evidence can result in considerable temporal differences for transitions (Fig. 5). For analyses relying on the temporal alignment of records (e.g. cross-correlation), age–depth model uncertainties should be considered using the ensemble of compatible age–depth models as described in, for example, Mudelsee et al. (2012), Rehfeld and Kurths (2014) and Hu et al. (2017).

5 Code and data availability

The database is available in SQL and CSV format from <https://doi.org/10.17864/1947.256> (Comas-Bru et al., 2020a). This dataset is licensed by the rights holder(s) under a Creative Commons Attribution 4.0 International License: <https://creativecommons.org/licenses/by/4.0/>. The code used for constructing the linear interpolation, linear regression, Bchron, Bacon, copRa and StalAge age–depth models is available at <https://github.com/paleovar/SISAL.AM> (last access: 23 July 2020; codes licensed by the right holder(s) under a GPL-3 license.). rBacon package (version 2.3.9.1) is available on CRAN (<https://cran.r-project.org/web/packages/rbacon/index.html>; last access: 31 January 2020; this package is licensed by the right holder(s) under a GPL-3 license.). The code used to construct the OxCal age–depth models and trim the ensemble output to the last 2000 iterations is available at <https://doi.org/10.5281/zenodo.3586280> (Amirnezhad-Mozhdehi and Comas-Bru, 2019). These codes are licensed by the right holder(s) under a Creative Commons Attribution 4.0 International. The ensembles are available at <https://doi.org/10.5281/zenodo.3816804> (Rehfeld et al., 2020). These codes are licensed by the right holder(s) under a Creative Commons Attribution 4.0 International. The workbook used to submit data to SISAL and the codes for its quality assessment are available at <https://doi.org/10.5281/zenodo.3631403> (Atsawawaranunt and Comas-Bru, 2020; scripts licensed by the right holder(s) under a Creative Commons Attribution 4.0 International.). The workbook is also available as a supplementary document of Comas-Bru and Harrison (2019) under a Creative Commons Attribution 4.0 International license. The codes to assess the dating table in SISALv2 are available at https://github.com/jensfohlmeister/QC_SISALv2_dating_

metadata (last access: 23 July 2020; licensed under a GPL-3 license) and <https://doi.org/10.5281/zenodo.3631443> (Comas-Bru et al., 2020b; licensed under a Creative Commons Attribution 4.0 License). Details on the quality control assessments are available in the Supplement.

6 Overview of database contents

SISALv2 contains 353 976 $\delta^{18}\text{O}$ and 200 613 $\delta^{13}\text{C}$ measurements from 673 individual speleothem records and 18 composite records from 293 cave sites (Table 5, Fig. 2; Comas-Bru et al., 2020a). There are 20 records included in SISALv2 that are identified as being superseded and linked to the newer records; their original datasets are included in the database for completeness. This is an improvement of 235 records from SISALv1b (Atsawawaranunt et al., 2019; Comas-Bru et al., 2019; Table 6). SISALv2 represents 72 % of the existing speleothem records identified by the SISAL working group and more than 3 times the number of speleothem records in the NCEI-NOAA repository ($n = 210$ as of November 2019; <https://www.ncdc.noaa.gov/data-access/paleoclimatology-data/datasets/speleothem> (last access: 20 October 2020), which is the one most commonly used by the speleothem community to make their data publicly available. SISALv2 also contains nine records that have not been published or are only available in PhD theses.

The published age–depth models of all speleothems are accessible in the *original_chronology* metadata table, and our standardized age–depth models are available in the *sisal_chronology* table for 512 speleothems. Temporal uncertainties are now provided for 79 % of the records in the SISAL database. This is a significantly larger number than in SISALv1b, where most age–depth models lacked temporal uncertainties. Most speleothem records show average $^{230}\text{Th}/\text{U}$ age errors between 100 and 1000 years (Fig. 6), which are only slightly changed by using age–depth modelling software. Nevertheless, when comparing the mean uncertainties of the $^{230}\text{Th}/\text{U}$ ages with those of their corresponding age–depth model, the slope between both parameters is smaller than 1. This indicates that age–depth models tend to reduce uncertainties, especially when dating errors are large, while they increase uncertainties when $^{230}\text{Th}/\text{U}$ age errors are small.

This second version of the SISAL database has an improved spatial coverage compared to SISALv1 (Atsawawaranunt et al., 2018b) and SISALv1b (Fig. 3; Atsawawaranunt et al., 2019). SISALv2 contains most published records from Oceania (80.2 %), Africa (73.7 %) and South America (77.6 %), but improvements are still possible in regions like the Middle East (42.3 %) and Asia (64.8 %; Table 6).

The temporal distribution of records for the past 2000 years is good, with 181 speleothems covering at least one-third of this period and 84 records covering the entire last 2000 years (–68 to 2000 years BP) with an average res-

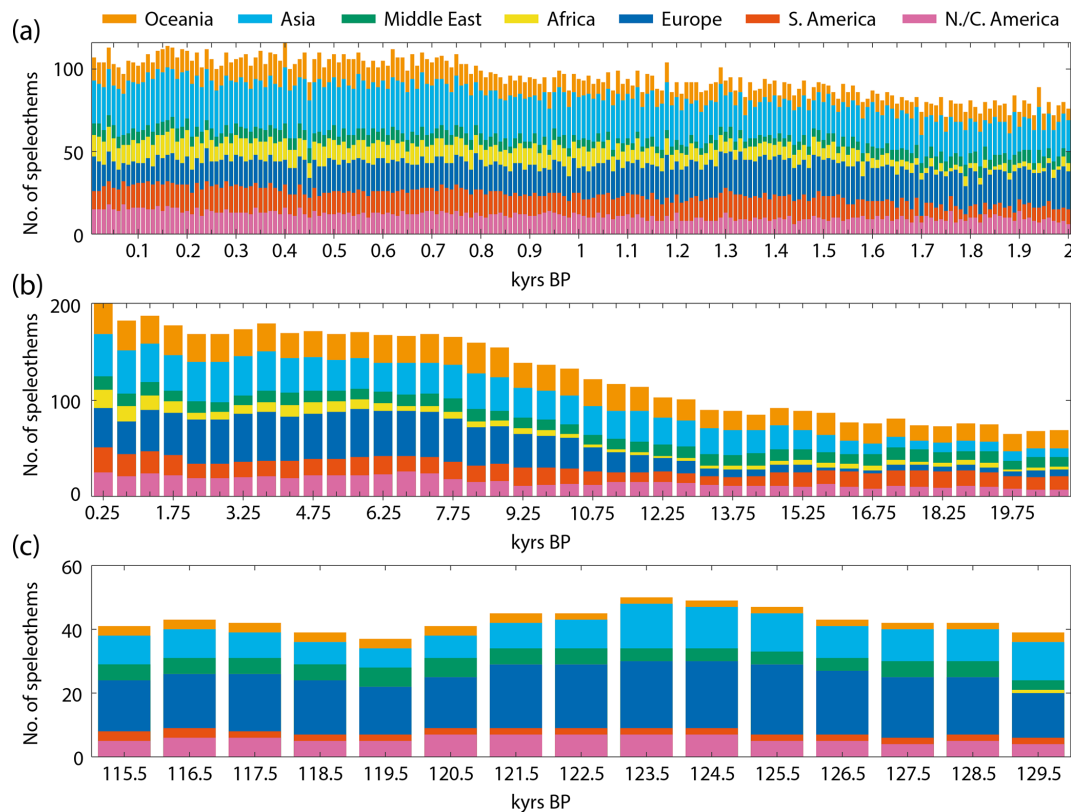


Figure 7. Global and regional temporal coverage of entities in the SISALv2. **(a)** Last 2000 years, with a bin size of 10 years; **(b)** last 21 000 years, with a bin size of 500 years; **(c)** the period between 115 000 and 130 000 years BP, with a bin size of 1000 years. BP refers to “before present”, where present is 1950 CE. Regions defined as in Table 7.

Table 6. Percentage of entities uploaded to the different versions of the SISAL database with respect to the number of records identified by the SISAL working group as of November 2019. The number of identified records includes potentially superseded speleothem records. Regions are defined as: Oceania ($-60^{\circ} < \text{Lat} < 0^{\circ}$; $90^{\circ} < \text{Long} < 180^{\circ}$), Asia ($0^{\circ} < \text{Lat} < 60^{\circ}$; $60^{\circ} < \text{Long} < 130^{\circ}$), Middle East ($7.6^{\circ} < \text{Lat} < 50^{\circ}$; $26^{\circ} < \text{Long} < 59^{\circ}$), Africa ($-45^{\circ} < \text{Lat} < 36.1^{\circ}$; $-30^{\circ} < \text{Long} < 60^{\circ}$; with records in the Middle East region removed), Europe ($36.7^{\circ} < \text{Lat} < 75^{\circ}$; $-30^{\circ} < \text{Long} < 30^{\circ}$; plus Gibraltar and Siberian sites), South America (S. Am.; $-60^{\circ} < \text{Lat} < 8^{\circ}$; $-150^{\circ} < \text{Long} < -30^{\circ}$), North and Central America (N./C. Am.; $8.1^{\circ} < \text{Lat} < 60^{\circ}$; $-150^{\circ} < \text{Long} < -50^{\circ}$).

Region	Version 1		Version 1b		Version 2	
	Entities	Sites	Entities	Sites	Entities	Sites
Oceania	47.7	36.7	56.8	51.0	80.2	69.4
Asia	36.2	28.8	41.1	33.3	64.8	48.5
Middle East	21.2	31.1	28.8	35.6	42.3	48.9
Africa	63.2	62.5	63.2	62.5	73.7	87.5
Europe	48.0	51.9	54.6	58.7	75.3	77.9
S. Am.	30.6	39.5	40.8	50.0	77.6	73.7
N./C. Am.	35.7	36.7	51.8	56.7	70.5	73.3

olution of 20 isotope measurements in every 100-year slice (Fig. 7a). There are 182 records that cover at least one-third of the Holocene (last 11 700 years BP), with 37 of these covering the whole period with at least one isotope measurement in every 500-year period (Fig. 7b). There are 84 entities during the deglaciation period (21 000 to 11 700 years BP) with at least one measurement in every 500-year time period (Fig. 7b). The Last Interglacial (130 000 to 115 000 years BP) is covered by 47 speleothem records that record at least one-third of this period with, on average, 25 isotope measurements in every 1000-year time slice (Fig. 7c).

This updated SISALv2 database now not only provides the basis for comparing a large number of speleothem-based environmental reconstructions on a regional to a global scale but also allows for comprehensive analyses of stable-isotope records on various timescales, from multi-decadal to orbital.

Supplement. The supplement related to this article is available online at: <https://doi.org/10.5194/essd-12-2579-2020-supplement>.

Team list. The following SISAL working group members contributed with either data or age-modelling advice to SISALv2: James Apaestegui (Instituto Geofísico del Perú, Lima, Peru), Lisa M. Baldini (School of Health and Life Sciences, Teesside University, Middlesbrough, UK), Shraddha Band (Geoscience Department, National Taiwan University, No. 1, Sect. 4, Roosevelt Road, Taipei 106, Taiwan), Maarten Blaauw (School of Natural and Built Environment, Queen's University Belfast, UK), Ronny Boch (Institute of Applied Geosciences, Graz University of Technology, Rechbauerstraße 12, 8010 Graz, Austria), Andrea Borsato (School of Environmental and Life Sciences, University of Newcastle, Callaghan 2308, NSW, Australia), Alexander Budzky (Institute for Geosciences, Johannes Gutenberg University Mainz, Johann-Joachim-Becher-Weg 21, 55128 Mainz, Germany), Maria Gracia Bustamante Rosell (Department of Geology and Environmental Science, University of Pittsburgh, USA), Sakonvan Chawchai (Department of Geology, Faculty of Science, Chulalongkorn University, Bangkok 10330, Thailand), Silviu Constantin (Emil Racovita Institute of Speleology, Bucharest, Romania, and Centro Nacional de Investigación sobre la Evolución Humana, CE-NIEH, Burgos, Spain), Rhawn Denniston (Department of Geology, Cornell College, Mount Vernon, IA 52314, USA), Virgil Dragusin (Emil Racovita Institute of Speleology, 010986, Strada Frumoașă 31, Bucharest, Romania), Russell Drysdale (School of Geography, University of Melbourne, Melbourne, Australia), Oana Dumitru (Karst Research Group, School of Geosciences, University of South Florida, 4202 E. Fowler Ave., NES 107, Tampa, FL 33620, USA), Amy Frappier (Department of Geosciences, Skidmore College, Saratoga Springs, New York, USA), Naveen Gandhi (Indian Institute of Tropical Meteorology, Homi Bhabha Road, Pashan, Pune-411008, India), Pawan Gautam (Centre for Earth, Ocean and Atmospheric Sciences, University of Hyderabad, India; now at Geological Survey of India, Northern Region, India), Li Hanying (Institute of Global Environmental Change, Xi'an Jiaotong University, China), Ilaria Isola (Istituto Nazionale di Geofisica e Vulcanologia, Pisa, Italy), Xiuyang Jiang (College of Geography Science, Fujian

Normal University, Fuzhou 350007, China), Zhao Jingyao (Institute of Global Environmental Change, Xi'an Jiaotong University, China), Kathleen Johnson (Dept. of Earth System Science, University of California, Irvine, 3200 Croul Hall, Irvine, CA 92697 USA), Vanessa Johnston (Research Centre of the Slovenian Academy of Sciences and Arts ZRC SAZU, Novi trg 2, Ljubljana, Slovenia), Gayatri Kathayat (Institute of Global Environmental Change, Xi'an Jiaotong University, China), Jennifer Klose (Institut für Geowissenschaften, Johannes Gutenberg University Mainz, Germany), Claire Krause (Geoscience Australia, Canberra, Australian Capital Territory, 2601, Australia), Matthew Lachniet (Department of Geoscience, University of Nevada Las Vegas, Las Vegas, NV 89154, USA), Amzad Laskar (Geosciences Division, Physical Research Laboratory, Navrangpura, Ahmedabad 380009, India), Stein-Erik Lauritzen (University of Bergen, Earth science, Norway), Nina Lončar (University of Zadar, Department of Geography, Trg Kneza Višeslava 9, 23000, Zadar, Croatia), Gina Moseley (Institute of Geology, University of Innsbruck, Innrain 52, 6020 Innsbruck, Austria), Allu C. Narayana (Centre for Earth, Ocean and Atmospheric Sciences, University of Hyderabad, India), Bogdan P. Onac (University of South Florida, School of Geosciences, 4202 E Fowler Ave, Tampa, FL 33620, USA and Emil Racoviță Institute of Speleology, Cluj-Napoca, Romania), Jacek Pawlak (Institute of Geological Sciences, Polish Academy of Sciences, 00-818, Twarda 51/55, Warsaw, Poland), Christopher Bronk Ramsey (Research Laboratory for Archaeology and the History of Art, Oxford University, Oxford, UK), Isabel Rivera-Collazo (Department of Anthropology and the Scripps Institution of Oceanography, UC San Diego, USA), Carlos Rossi (Dept. Petrología y Geoquímica, Facultad de Ciencias Geológicas, Universidad Complutense, Madrid, Spain), Peter J. Rowe (School of Environmental Sciences, University of East Anglia, NR4 7TJ, Norwich Research Park, Norwich, UK), Nicolás M. Strikis (Department of Geochemistry, Universidade Federal Fluminense, Niterói, Brazil), Liangcheng Tan (State Key Laboratory of Loess and Quaternary Geology, Institute of Earth Environment, Chinese Academy of Sciences, Xi'an 710075, China), Sophie Verheyden (Politique scientifique fédérale belge BELSPO, Bvd. Simon Bolivar 30, 1000 Brussels, Belgium), Hubert Vonhof (Max Planck Institute for Chemistry, Mainz, Germany), Michael Weber (Johannes Gutenberg University Mainz, Germany), Kathleen Wendt (Institute of Geology, University of Innsbruck, Austria), Paul Wilcox (Institute of Geology, University of Innsbruck, Austria), Amos Winter (Dept. of Earth and Environmental Systems, Indiana State University, USA), Jiangying Wu (School of Geography, Nanjing Normal University, Nanjing, China), Peter Wynn (Lancaster Environment Centre, University of Lancaster, Lancaster, LA1 4YQ, UK) and Madhusudan G. Yadava (Geosciences Division, Physical Research Laboratory, Navrangpura, Ahmedabad 380009, India).

Author contributions. LCB is the coordinator of the SISAL working group. LCB, SPH and KR designed the new version of the database. KR coordinated the construction of the new age–depth models except OxCal. All age–depth models except OxCal were run by CR and KR. LCB coordinated the construction of the OxCal age–depth models, which were run by SAM and LCB. LCB implemented the changes in the v2 of the database with the assistance of KA, SMA, YAB, AB, YB, MB, AC, MD, AD, BD, IGH, JH, NK, ZK, FAL, AL, BM, VFN, JO, CPM, NSc, NSi, BMW, SW and HZ

coordinated the regional data collection and the age model screening. SFMB, MB and DS provided support for COPRA, Bacon and StalAge, respectively. JF assisted in the quality control procedure of the SISAL database. Figures 1, 4 and 5 were created by CR and KR. Figures 2, 3 and 6 were created by LCB. All authors listed as “SISAL working group members” provided data for this version of the database and/or helped to complete data entry. The first draft of the paper was written by LCB with input by KR and SPH, and all authors contributed to the final version.

Competing interests. The authors declare that they have no conflict of interest.

Acknowledgements. This study was undertaken by SISAL (Speleothem Isotopes Synthesis and Analysis), a working group of the Past Global Changes (PAGES) project, which in turn received support from the Swiss Academy of Sciences and the Chinese Academy of Sciences. We thank SISAL members who contributed their published data to the database and provided additional information when necessary. We thank all experts who engaged in the age–depth model evaluation. The authors would like to acknowledge Avner Ayalon, Jordi López, Bahadur Singh Kotlia and Dennis Rupprecht.

Financial support. The design and creation of v2 of the database were supported by funding to Sandy P. Harrison from the ERC-funded project GC2.0 (Global Change 2.0: Unlocking the past for a clearer future; grant no. 694481) and the Geological Survey Ireland Short Call 2017 (Developing a toolkit for model evaluation using speleothem isotope data; grant no. 2017-SC-056) award to Laia Comas-Bru. Sandy P. Harrison and Laia Comas-Bru received additional support from the ERC-funded project GC2.0 and from the JPI-Belmont project “Palaeo-Constraints on Monsoon Evolution and Dynamics (PACMEDY)” through the UK Natural Environmental Research Council (NERC). Laia Comas-Bru and Belen Martrat received support from the CSIC scientific international collaboration programme I-LINKA20102 IBCC-lo2k. Kira Rehfeld and Denis Scholz acknowledge support by the Deutsche Forschungsgemeinschaft (DFG; codes RE3994/2-1 and SCHO 1274/11-1).

Review statement. This paper was edited by Thomas Blunier and reviewed by Oliver Bothe and Judson W. Partin.

References

- Ait Brahim, Y., Wassenburg, J. A., Cruz, F. W., Sifeddine, A., Scholz, D., Bouchaou, L., Dassie, E. P., Jochum, K. P., Edwards, R. L., and Cheng, H.: Multi-decadal to centennial hydroclimate variability and linkage to solar forcing in the Western Mediterranean during the last 1000 years, *Sci. Rep.*, 8, 174466, <https://doi.org/10.1038/s41598-018-35498-x>, 2018.
- Ait Brahim, Y., Wassenburg, J. A., Sha, L., Cruz, F. W., Deininger, M., Sifeddine, A., Bouchaou, L., Spötl, C., Edwards, R. L., and Cheng, H.: North Atlantic Ice-Rafting, Ocean and Atmospheric Circulation During the Holocene: Insights From Western Mediterranean Speleothems, *Geophys. Res. Lett.*, 46, GL082405, <https://doi.org/10.1029/2019GL082405>, 2019.
- Amin Al-Manmi, D. A. M., Ismaeel, S. B., and Altaweel, M.: Reconstruction of palaeoclimate in Shalaih Cave, SE of Sangaw, Kurdistan Province of Iraq, *Palaeogeogr. Palaeoclimatol.*, 524, 262–272, <https://doi.org/10.1016/j.palaeo.2019.03.044>, 2019.
- Amirnezhad-Mozhdehi, S. and Comas-Bru, L.: MATLAB scripts to produce OxCal chronologies for SISAL database (scripts V1) (Version 1.0), Zenodo, <https://doi.org/10.5281/zenodo.3586280>, 2019.
- Apaeestegui, J., Cruz, F. W., Vuille, M., Fohlmeister, J., Espinoza, J. C., Sifeddine, A., Strikis, N., Guyot, J. L., Ventura, R., Cheng, H., and Edwards, R. L.: Precipitation changes over the eastern Bolivian Andes inferred from speleothem ($\delta\text{O}-18$) records for the last 1400 years, *Earth Planet. Sc. Lett.*, 494, 124–134, <https://doi.org/10.1016/j.epsl.2018.04.048>, 2018.
- Asmerom, Y., Polyak, V., Burns, S., and Rasmussen, J.: Solar forcing of Holocene climate: New insights from a speleothem record, southwestern United States, *Geology*, 35, 1–4, <https://doi.org/10.1130/G22865A.1>, 2007.
- Asmerom, Y., Polyak, V. J., Rasmussen, J. B. T., Burns, S. J., and Lachniet, M.: Multidecadal to multicentury scale collapses of Northern Hemisphere monsoons over the past millennium, *P. Natl. Acad. Sci. USA*, 110, 9651–9656, <https://doi.org/10.1073/pnas.1214870110>, 2013.
- Atsawawaranunt, K., Comas-Bru, L., Amirnezhad Mozhdehi, S., Deininger, M., Harrison, S. P., Baker, A., Boyd, M., Kaushal, N., Ahmad, S. M., Ait Brahim, Y., Arienzo, M., Bajo, P., Braun, K., Burstyn, Y., Chawchai, S., Duan, W., Hatvani, I. G., Hu, J., Kern, Z., Labuhn, I., Lachniet, M., Lechleitner, F. A., Lorey, A., Pérez-Mejías, C., Pickering, R., Scroton, N., and SISAL Working Group Members: The SISAL database: a global resource to document oxygen and carbon isotope records from speleothems, *Earth Syst. Sci. Data*, 10, 1687–1713, <https://doi.org/10.5194/essd-10-1687-2018>, 2018a.
- Atsawawaranunt, K., Harrison, S., and Comas-Bru, L.: SISAL (Speleothem Isotopes Synthesis and AnaLysis Working Group) database Version 1.0, University of Reading, Dataset, <https://doi.org/10.17864/1947.147>, 2018b.
- Atsawawaranunt, K., Harrison, S., and Comas-Bru, L.: SISAL (Speleothem Isotopes Synthesis and AnaLysis Working Group) database Version 1b, University of Reading, Dataset, <https://doi.org/10.17864/1947.189>, 2019.
- Badertscher, S., Fleitmann, D., Cheng, H., Edwards, R. L., Gökür, O. M., Zumbühl, A., Leuenberger, M., and Tüysüz, O.: Pleistocene water intrusions from the Mediterranean and Caspian seas into the Black Sea, *Nat. Geosci.*, 4, 236–239, <https://doi.org/10.1038/ngeo1106>, 2011.
- Baldini, L. M., McDermott, F., Baldini, J. U. L., Arias, P., Cueto, M., Fairchild, I. J., Hoffmann, D. L., Matthey, D. P., Muller, W., Nita, D. C., Ontanon, R., Garcia-Monco, C., and Richards, D. A.: Regional temperature, atmospheric circulation, and sea-ice variability within the Younger Dryas Event constrained using a speleothem from northern Iberia, *Earth Planet. Sc. Lett.*, 419, 101–110, <https://doi.org/10.1016/j.epsl.2015.03.015>, 2015.
- Baldini, L. M., Baldini, J. U. L., McDermott, F., Arias, P., Cueto, M., Fairchild, I. J., Hoffmann, D. L., Matthey, D. P.,

- Müller, W., Nita, D. C., Ontañón, R., García-Moncó, C., and Richards, D. A.: North Iberian temperature and rainfall seasonality over the Younger Dryas and Holocene, *Quaternary Sci. Rev.*, 226, 105998, <https://doi.org/10.1016/j.quascirev.2019.105998>, 2019.
- Band, S., Yadava, M. G., Lone, M. A., Shen, C. C., Sree, K., and Ramesh, R.: High-resolution mid-Holocene Indian Summer Monsoon recorded in a stalagmite from the Kotumsar Cave, Central India, *Quatern. Int.*, 479, 19–24, <https://doi.org/10.1016/j.quaint.2018.01.026>, 2018.
- Bar-Matthews, M., Ayalon, A., Gilmour, M., Matthews, A., and Hawkesworth, C. J.: Sea–land oxygen isotopic relationships from planktonic foraminifera and speleothems in the Eastern Mediterranean region and their implication for paleorainfall during interglacial intervals, *Geochim. Cosmochim. Ac.*, 67, 3181–3199, [https://doi.org/10.1016/S0016-7037\(02\)01031-1](https://doi.org/10.1016/S0016-7037(02)01031-1), 2003.
- Blaauw, M.: Methods and code for “classical” age-modelling of radiocarbon sequences, *Quat. Geochronol.*, 5, 512–518, <https://doi.org/10.1016/j.quageo.2010.01.002>, 2010.
- Blaauw, M. and Christen, J. A.: Flexible paleoclimate age-depth models using an autoregressive gamma process, *Bayesian Anal.*, 6, 457–474, <https://doi.org/10.1214/11-ba618>, 2011.
- Blaauw, M., Christen, J. A., Vazquez, J. E., Belding, T., Theiler, J., Gough, B., and Karney, C.: rbacon: Age-depth modelling using Bayesian statistics: R package, version 2.3.9.1, last access: <https://cran.r-project.org/web/packages/rbacon/>, last access: 20 October 2019.
- Braun, K., Nehme, C., Pickering, R., Rogerson, M., and Scroxton, N.: A Window into Africa’s Past Hydroclimates: The SISAL_v1 Database Contribution, *Quaternary*, 2, 4, <https://doi.org/10.3390/quat2010004>, 2019a.
- Braun, K., Bar-Matthews, M., Matthews, A., Ayalon, A., Cowling, R. M., Karkanas, P., Fisher, E. C., Dyez, K., Zilberman, T., and Marean, C. W.: Late Pleistocene records of speleothem stable isotopic compositions from Pinnacle Point on the South African south coast, *Quaternary Res.*, 91, 265–288, <https://doi.org/10.1017/qua.2018.61>, 2019b.
- Breitenbach, S. F. M., Rehfeld, K., Goswami, B., Baldini, J. U. L., Ridley, H. E., Kennett, D. J., Prufer, K. M., Aquino, V. V., Asmerom, Y., Polyak, V. J., Cheng, H., Kurths, J., and Marwan, N.: CONSTRUCTING Proxy Records from Age models (CO-PRA), *Clim. Past*, 8, 1765–1779, <https://doi.org/10.5194/cp-8-1765-2012>, 2012.
- Breitenbach, S. F. M., Plessen, B., Waltgenbach, S., Tjallingii, R., Leonhardt, J., Jochum, K. P., Meyer, H., Goswami, B., Marwan, N., and Scholz, D.: Holocene interaction of maritime and continental climate in Central Europe: New speleothem evidence from Central Germany, *Global Planet. Change*, 176, 144–161, <https://doi.org/10.1016/J.GLOPLACHA.2019.03.007>, 2019.
- Bronk Ramsey, C.: Deposition models for chronological records, *Quaternary Sci. Rev.*, 27, 42–60, <https://doi.org/10.1016/j.quascirev.2007.01.019>, 2008.
- Bronk Ramsey, C.: Bayesian analysis of radiocarbon dates, *Radiocarbon*, 51, 337–360, <https://doi.org/10.1017/S0033822200033865>, 2009.
- Bronk Ramsey, C. and Lee, S.: Recent and planned developments of the program OxCal, *Radiocarbon*, 55, 720–730, https://doi.org/10.2458/azu_js_rc.55.16215, 2013.
- Budsky, A., Scholz, D., Wassenburg, J. A., Mertz-Kraus, R., Spötl, C., Riechelmann, D. F. C., Gibert, L., Jochum, K. P., and Andreae, M. O.: Speleothem $\delta^{13}\text{C}$ record suggests enhanced spring/summer drought in south-eastern Spain between 9.7 and 7.8 ka – A circum-Western Mediterranean anomaly?, *Holocene*, 29, 1113–1133, <https://doi.org/10.1177/0959683619838021>, 2019.
- Burns, S. J., Fleitmann, D., Matter, A., Kramers, J., and Al-Subbary, A. A.: Indian Ocean Climate and an Absolute Chronology over Dansgaard/Oeschger Events 9 to 13, *Science*, 301, 1365–1367, <https://doi.org/10.1126/science.1086227>, 2003.
- Burns, S. J., Fleitmann, D., Matter, A., Kramers, J., and Al-Subbary, A. A.: Corrections and Clarifications, *Science*, 305, 1567a–1567a, <https://doi.org/10.1126/science.305.5690.1567a>, 2004.
- Burns, S. J., Welsh, L. K., Scroxton, N., Cheng, H., and Edwards, R. L.: Millennial and orbital scale variability of the South American Monsoon during the penultimate glacial period, *Sci. Rep.*, 9, 1234, <https://doi.org/10.1038/s41598-018-37854-3>, 2019.
- Burstyn, Y., Martrat, B., Lopez, F. J., Iriarte, E., Jacobson, J. M., Lone, A. M., and Deininger, M.: Speleothems from the Middle East: An Example of Water Limited Environments in the SISAL Database, *Quaternary*, 2, 16, <https://doi.org/10.3390/quat2020016>, 2019.
- Cai, Y. J., Chiang, J. C. H., Breitenbach, S. F. M., Tan, L. C., Cheng, H., Edwards, R. L., and An, Z. S.: Holocene moisture changes in western China, Central Asia, inferred from stalagmites, *Quaternary Sci. Rev.*, 158, 15–28, <https://doi.org/10.1016/j.quascirev.2016.12.014>, 2017.
- Carolin, S. A., Cobb, K. M., Lynch-Stieglitz, J., Moerman, J. W., Partin, J. W., Lejau, S., Malang, J., Clark, B., Tuen, A. A., and Adkins, J. F.: Northern Borneo stalagmite records reveal West Pacific hydroclimate across MIS 5 and 6, *Earth Planet. Sc. Lett.*, 439, 182–193, <https://doi.org/10.1016/j.epsl.2016.01.028>, 2016.
- Carolin, S. A., Walker, R. T., Day, C. C., Ersek, V., Sloan, R. A., Dee, M. W., Talebian, M., and Henderson, G. M.: Precise timing of abrupt increase in dust activity in the Middle East coincident with 4.2 ka social change, *P. Natl. Acad. Sci. USA*, 116, 67–72, <https://doi.org/10.1073/PNAS.1808103115>, 2019.
- Cheng, H., Edwards, R. L., Wan, Y. J., Ko, X. G., Ming, Y. F., Kelly, M. J., Wang, X. F., Gallup, C. D., and Liu, W. G.: A penultimate glacial monsoon record from Hulu Cave and two-phase glacial terminations, *Geology*, 34, 217–220, <https://doi.org/10.1130/g22289.1>, 2006.
- Cheng, H., Fleitmann, D., Edwards, R. L., Wang, X., Cruz, F. W., Auler, A. S., Mangini, A., Wang, Y., Kong, X., Burns, S. J., and Matter, A.: Timing and structure of the 8.2 kyr B.P. event inferred from $\delta^{18}\text{O}$ records of stalagmites from China, Oman, and Brazil, *Geology*, 37, 1007–1010, <https://doi.org/10.1130/G30126A.1>, 2009.
- Cheng, H., Sinha, A., Cruz, F. W., Wang, X., Edwards, R. L., d’Horta, F. M., Ribas, C. C., Vuille, M., Stott, L. D., and Auler, A. S.: Climate change patterns in Amazonia and biodiversity, *Nat. Commun.*, 4, 1411, <https://doi.org/10.1038/ncomms2415>, 2013.
- Cheng, H., Springer, G. S., Sinha, A., Hardt, B. F., Yi, L., Li, H., Tian, Y., Li, X., Rowe, H. D., Kathayat, G., Ning, Y., and Edwards, R. L.: Eastern North American climate in

- phase with fall insolation throughout the last three glacial-interglacial cycles, *Earth Planet. Sc. Lett.*, 522, 125–134, <https://doi.org/10.1016/j.epsl.2019.06.029>, 2019.
- Columbu, A., Spötl, C., De Waele, J., Yu, T.-L., Shen, C.-C., and Gázquez, F.: A long record of MIS 7 and MIS 5 climate and environment from a western Mediterranean speleothem (SW Sardinia, Italy), *Quaternary Sci. Rev.*, 220, 230–243, <https://doi.org/10.1016/J.QUASCIREV.2019.07.023>, 2019.
- Comas-Bru, L. and Harrison, S. P.: SISAL: Bringing added value to speleothem research, *Quaternary*, 2, 7, <https://doi.org/10.3390/quat2010007>, 2019.
- Comas-Bru, L., Harrison, S. P., Werner, M., Rehfeld, K., Scroxton, N., Veiga-Pires, C., and SISAL working group members: Evaluating model outputs using integrated global speleothem records of climate change since the last glacial, *Clim. Past*, 15, 1557–1579, <https://doi.org/10.5194/cp-15-1557-2019>, 2019.
- Comas-Bru, L., Atsawawaranunt, K., Harrison, S. P. and SISAL Working Group members: SISAL (Speleothem Isotopes Synthesis and AnaLysis Working Group) database version 2.0, University of Reading, Dataset, <https://doi.org/10.17864/1947.256>, 2020a.
- Comas-Bru, L., Deininger, M., Fohlmeister, J., Baker, A., McDermott, F., and Scholz, D.: Quality control of the dating information table in the SISAL database, Zenodo, <https://doi.org/10.5281/zenodo.3631443>, 2020b.
- Cruz, F. W., Burns, S. J., Karmann, I., Sharp, W. D., and Vuille, M.: Reconstruction of regional atmospheric circulation features during the late Pleistocene in subtropical Brazil from oxygen isotope composition of speleothems, *Earth Planet. Sc. Lett.*, 248, 495–507, <https://doi.org/10.1016/J.EPSL.2006.06.019>, 2006.
- Czuppon, G., Demeny, A., Leel-Ossy, S., Ovari, M., Molnar, M., Stieber, J., Kiss, K., Karman, K., Suranyi, G., and Haszpra, L.: Cave monitoring in the Beke and Baradla caves (Northeastern Hungary): implications for the conditions for the formation cave carbonates, *Int. J. Speleol.*, 47, 13–28, <https://doi.org/10.5038/1827-806x.47.1.2110>, 2018.
- Deininger, M., Ward, M. B., Novello, F. V., and Cruz, W. F.: Late Quaternary Variations in the South American Monsoon System as Inferred by Speleothems – New Perspectives Using the SISAL Database, *Quaternary*, 2, 6, <https://doi.org/10.3390/quat2010006>, 2019.
- Demény, A., Kern, Z., Németh, A., Frisia, S., Hatvani, I. G., Czuppon, G., Leél-Őssy, S., Molnár, M., Óvári, M., Surányi, G., Gilli, A., Wu, C.-C., and Shen, C.-C.: North Atlantic influences on climate conditions in East-Central Europe in the late Holocene reflected by flowstone compositions, *Quatern. Int.*, 512, 99–112, <https://doi.org/10.1016/J.QUAINT.2019.02.014>, 2019.
- Denniston, R. F., Asmerom, Y., Lachniet, M., Polyak, V. J., Hope, P., An, N., Rodzinyak, K., and Humphreys, W. F.: A Last Glacial Maximum through middle Holocene stalagmite record of coastal Western Australia climate, *Quaternary Sci. Rev.*, 77, 101–112, <https://doi.org/10.1016/j.quascirev.2013.07.002>, 2013a.
- Denniston, R. F., Wyrwoll, K.-H., Polyak, V. J., Brown, J. R., Asmerom, Y., Wanamaker, A. D., LaPointe, Z., Ellerböck, R., Barthelmes, M., Cleary, D., Cugley, J., Woods, D., and Humphreys, W. F.: A Stalagmite record of Holocene Indonesian–Australian summer monsoon variability from the Australian tropics, *Quaternary Sci. Rev.*, 78, 155–168, <https://doi.org/10.1016/J.QUASCIREV.2013.08.004>, 2013b.
- Denniston, R. F., Asmerom, Y., Polyak, V. J., Wanamaker, A. D., Ummenhofer, C. C., Humphreys, W. F., Cugley, J., Woods, D., and Lucker, S.: Decoupling of monsoon activity across the northern and southern Indo-Pacific during the Late Glacial, *Quaternary Sci. Rev.*, 176, 101–105, <https://doi.org/10.1016/J.QUASCIREV.2017.09.014>, 2017.
- Denniston, R. F., Houts, A. N., Asmerom, Y., Wanamaker Jr., A. D., Haws, J. A., Polyak, V. J., Thatcher, D. L., Altan-Ochir, S., Borowske, A. C., Breitenbach, S. F. M., Ummenhofer, C. C., Regala, F. T., Benedetti, M. M., and Bicho, N. F.: A stalagmite test of North Atlantic SST and Iberian hydroclimate linkages over the last two glacial cycles, *Clim. Past*, 14, 1893–1913, <https://doi.org/10.5194/cp-14-1893-2018>, 2018.
- Dong, J., Shen, C.-C., Kong, X., Wu, C.-C., Hu, H.-M., Ren, H., and Wang, Y.: Rapid retreat of the East Asian summer monsoon in the middle Holocene and a millennial weak monsoon interval at 9 ka in northern China, *J. Asian Earth Sci.*, 151, 31–39, <https://doi.org/10.1016/J.JSEAES.2017.10.016>, 2018.
- Dumitru, O. A., Onac, B. P., Polyak, V. J., Wynn, J. G., Asmerom, Y., and Fornos, J. J.: Climate variability in the western Mediterranean between 121 and 67 ka derived from a Mallorcan speleothem record, *Palaeogeogr. Palaeoclimatol.*, 506, 128–138, <https://doi.org/10.1016/j.palaeo.2018.06.028>, 2018.
- El-Shenawy, M. I., Kim, S. T., Schwarcz, H. P., Asmerom, Y., and Polyak, V. J.: Speleothem evidence for the greening of the Sahara and its implications for the early human dispersal out of sub-Saharan Africa, *Quaternary Sci. Rev.*, 188, 67–76, <https://doi.org/10.1016/j.quascirev.2018.03.016>, 2018.
- Fleitmann, D., Cheng, H., Badertscher, S., Edwards, R. L., Mudelsee, M., Göktürk, O. M., Fankhauser, A., Pickering, R., Raible, C. C., Matter, A., Kramers, J., and Tüysüz, O.: Timing and climatic impact of Greenland interstadials recorded in stalagmites from northern Turkey, *Geophys. Res. Lett.*, 36, L19707–L19707, <https://doi.org/10.1029/2009GL040050>, 2009.
- Flohr, P., Fleitmann, D., Zorita, E., Sadekov, A., Cheng, H., Bosomworth, M., Edwards, L., Matthews, W., and Matthews, R.: Late Holocene droughts in the Fertile Crescent recorded in a speleothem from northern Iraq, *Geophys. Res. Lett.*, 44, 1528–1536, <https://doi.org/10.1002/2016GL071786>, 2017.
- Frappier, A., Sahagian, D., González, L. A., and Carpenter, S. J.: El Niño Events Recorded by Stalagmite Carbon Isotopes, *Science*, 298, 565–565, <https://doi.org/10.1126/science.1076446>, 2002.
- Frappier, A. B., Sahagian, D., Carpenter, S. J., Gonzalez, L. A., and Frappier, B. R.: Stalagmite stable isotope record of recent tropical cyclone events, *Geology*, 35, 111–114, <https://doi.org/10.1130/g23145a.1>, 2007.
- Gautam, P. K., Narayana, A. C., Band, S. T., Yadava, M. G., Ramesh, R., Wu, C.-C., and Shen, C.-C.: High-resolution reconstruction of Indian summer monsoon during the Bølling-Allerød from a central Indian stalagmite, *Palaeogeogr. Palaeoclimatol.*, 514, 567–576, <https://doi.org/10.1016/J.PALAEO.2018.11.006>, 2019.
- Göktürk, O. M., Fleitmann, D., Badertscher, S., Cheng, H., Edwards, R. L., Leuenberger, M., Fankhauser, A., Tüysüz, O., and Kramers, J.: Climate on the southern Black Sea coast during the Holocene: implications from the Sofu-

- lar Cave record, *Quaternary Sci. Rev.*, 30, 2433–2445, <https://doi.org/10.1016/J.QUASCIREV.2011.05.007>, 2011.
- Goldscheider, N., Chen, Z., Auler, A. S., Bakalowicz, M., Broda, S., Drew, D., Hartmann, J., Jiang, G., Moosdorf, N., Stevanovic, Z., and Veni, G.: Global distribution of carbonate rocks and karst water resources, *Hydrogeol. J.*, 28, 1661–1677, <https://doi.org/10.1007/s10040-020-02139-5>, 2020.
- Haslett, J. and Parnell, A.: A simple monotone process with application to radiocarbon-dated depth chronologies, *J. R. Stat. Soc. C-Appl.*, 57, 399–418, <https://doi.org/10.1111/j.1467-9876.2008.00623.x>, 2008.
- Hu, J., Emile-Geay, J., and Partin, J.: Correlation-based interpretations of paleoclimate data—where statistics meet past climates, *Earth Planet. Sc. Lett.*, 459, 362–371, <https://doi.org/10.1016/j.epsl.2016.11.048>, 2017.
- Huguet, C., Routh, J., Fietz, S., Lone, M. A., Kalpana, M. S., Ghosh, P., Mangini, A., Kumar, V., and Rangarajan, R.: Temperature and Monsoon Tango in a Tropical Stalagmite: Last Glacial-Interglacial Climate Dynamics, *Sci. Rep.*, 8, 5386, <https://doi.org/10.1038/s41598-018-23606-w>, 2018.
- Isola, I., Zanchetta, G., Drysdale, R. N., Regattieri, E., Bini, M., Bajo, P., Hellstrom, J. C., Banerjee, I., Lionello, P., Woodhead, J., and Greig, A.: The 4.2 ka event in the central Mediterranean: new data from a Corchia speleothem (Apuan Alps, central Italy), *Clim. Past*, 15, 135–151, <https://doi.org/10.5194/cp-15-135-2019>, 2019.
- Jamieson, R. A., Baldini, J. U. L., Frappier, A. B., and Müller, W.: Volcanic ash fall events identified using principal component analysis of a high-resolution speleothem trace element dataset, *Earth Planet. Sc. Lett.*, 426, 36–45, <https://doi.org/10.1016/J.EPSL.2015.06.014>, 2015.
- Jex, C. N., Baker, A., Fairchild, I. J., Eastwood, W. J., Leng, M. J., Sloane, H. J., Thomas, L., and Bekaroglu, E.: Calibration of speleothem delta O-18 with instrumental climate records from Turkey, *Global Planet. Change*, 71, 207–217, <https://doi.org/10.1016/j.gloplacha.2009.08.004>, 2010.
- Jex, C. N., Baker, A., Eden, J. M., Eastwood, W. J., Fairchild, I. J., Leng, M. J., Thomas, L., and Sloane, H. J.: A 500 yr speleothem-derived reconstruction of late autumn–winter precipitation, northeast Turkey, *Quaternary Res.*, 75, 399–405, <https://doi.org/10.1016/j.yqres.2011.01.005>, 2011.
- Jex, C. N., Phipps, S. J., Baker, A., and Bradley, C.: Reducing uncertainty in the climatic interpretations of speleothem delta O-18, *Geophys. Res. Lett.*, 40, 2259–2264, <https://doi.org/10.1002/grl.50467>, 2013.
- Jiang, X., He, Y., Shen, C., Kong, X., Li, Z., and Chang, Y.: Stalagmite-inferred Holocene precipitation in northern Guizhou Province, China, and asynchronous termination of the Climatic Optimum in the Asian monsoon territory, *Chinese Sci. Bull.*, 57, 795–801, <https://doi.org/10.1007/s11434-011-4848-6>, 2012.
- Jiang, X., He, Y., Shen, C.-C., Li, Z., and Lin, K.: Replicated stalagmite-inferred centennial-to decadal-scale monsoon precipitation variability in southwest China since the mid Holocene, *Holocene*, 23, 841–849, <https://doi.org/10.1177/0959683612471986>, 2013.
- Jo, K.-n., Yi, S., Lee, J.-Y., Woo, K. S., Cheng, H., Edwards, L. R., and Kim, S.-T.: 1000-Year Quasi-Periodicity of Weak Monsoon Events in Temperate Northeast Asia since the Mid-Holocene, *Sci. Rep.*, 7, 15196, <https://doi.org/10.1038/s41598-017-15566-4>, 2017.
- Johnson, K. R., Ingram, B. L., Sharp, W. D., and Zhang, P. Z.: East Asian summer monsoon variability during Marine Isotope Stage 5 based on speleothem $\delta^{18}\text{O}$ records from Wanxiang Cave, central China, *Palaeogeogr. Palaeoclimatol.*, 236, 5–19, <https://doi.org/10.1016/j.palaeo.2005.11.041>, 2006.
- Kanner, L. C., Burns, S. J., Cheng, H., and Edwards, R. L.: High-Latitude Forcing of the South American Summer Monsoon During the Last Glacial, *Science*, 335, 570–573, <https://doi.org/10.1126/science.1213397>, 2012.
- Kanner, L. C., Burns, S. J., Cheng, H., Edwards, R. L., and Vuille, M.: High-resolution variability of the South American summer monsoon over the last seven millennia: insights from a speleothem record from the central Peruvian Andes, *Quaternary Sci. Rev.*, 75, 1–10, <https://doi.org/10.1016/j.quascirev.2013.05.008>, 2013.
- Kathayat, G., Cheng, H., Sinha, A., Yi, L., Li, X. L., Zhang, H. W., Li, H. Y., Ning, Y. F., and Edwards, R. L.: The Indian monsoon variability and civilization changes in the Indian subcontinent, *Science Advances*, 3, e1701296, <https://doi.org/10.1126/sciadv.1701296>, 2017.
- Kathayat, G., Cheng, H., Sinha, A., Berkelhammer, M., Zhang, H., Duan, P., Li, H., Li, X., Ning, Y., and Edwards, R. L.: Evaluating the timing and structure of the 4.2 ka event in the Indian summer monsoon domain from an annually resolved speleothem record from Northeast India, *Clim. Past*, 14, 1869–1879, <https://doi.org/10.5194/cp-14-1869-2018>, 2018.
- Kaushal, N., Breitenbach, F. M. S., Lechleitner, A. F., Sinha, A., Tewari, C. V., Ahmad, M. S., Berkelhammer, M., Band, S., Yadava, M., Ramesh, R., and Henderson, M. G.: The Indian Summer Monsoon from a Speleothem $\delta^{18}\text{O}$ Perspective – A Review, *Quaternary*, 1, 29, <https://doi.org/10.3390/quat1030029>, 2018.
- Kern, Z., Demény, A., Perşoiu, A., and Hatvani, G. I.: Speleothem Records from the Eastern Part of Europe and Turkey – Discussion on Stable Oxygen and Carbon Isotopes, *Quaternary*, 2, 31, <https://doi.org/10.3390/quat2030031>, 2019.
- Krause, C. E., Gagan, M. K., Dunbar, G. B., Hantoro, W. S., Hellstrom, J. C., Cheng, H., Edwards, R. L., Suwargadi, B. W., Abram, N. J., and Rifai, H.: Spatio-temporal evolution of Australasian monsoon hydroclimate over the last 40,000 years, *Earth Planet. Sc. Lett.*, 513, 103–112, <https://doi.org/10.1016/J.EPSL.2019.01.045>, 2019.
- Lachniet, M. S., Asmerom, Y., Burns, S. J., Patterson, W. P., Polyak, V. J., and Seltzer, G. O.: Tropical response to the 8200 yr BP cold event? Speleothem isotopes indicate a weakened early Holocene monsoon in Costa Rica, *Geology*, 32, 957–960, <https://doi.org/10.1130/g20797.1>, 2004.
- Lachniet, M. S., Johnson, L., Asmerom, Y., Burns, S. J., Polyak, V., Patterson, W. P., Burt, L., and Azouz, A.: Late Quaternary moisture export across Central America and to Greenland: evidence for tropical rainfall variability from Costa Rican stalagmites, *Quaternary Sci. Rev.*, 28, 3348–3360, <https://doi.org/10.1016/J.QUASCIREV.2009.09.018>, 2009.
- Laskar, A. H., Yadava, M. G., Ramesh, R., Polyak, V. J., and Asmerom, Y.: A 4 kyr stalagmite oxygen isotopic record of the past Indian Summer Monsoon in the Andaman Islands, *Geochem., Geophys., Geosys.*, 14, 3555–3566, <https://doi.org/10.1002/ggge.20203>, 2013.

- Lauritzen, S.-E., and Onac, B. P.: Isotopic Stratigraphy of a Last Interglacial Stalagmite from Northwestern Romania: Correlation with the Deep-Sea record and Northern-Latitude Speleothem, *J. Cave Karst Stud.*, 61, 22–30, 1999.
- Lechleitner, F. A., Amirnezhad-Mozhdehi, S., Columbu, A., Comas-Bru, L., Labuhn, I., Pérez-Mejías, C., and Rehfeld, K.: The Potential of Speleothems from Western Europe as Recorders of Regional Climate: A Critical Assessment of the SISAL Database, *Quaternary*, 1, 30, <https://doi.org/10.3390/quat1030030>, 2018.
- Li, H., Cheng, H., Sinha, A., Kathayat, G., Spötl, C., André, A. A., Meunier, A., Biswas, J., Duan, P., Ning, Y., and Edwards, R. L.: Hydro-climatic variability in the southwestern Indian Ocean between 6000 and 3000 years ago, *Clim. Past*, 14, 1881–1891, <https://doi.org/10.5194/cp-14-1881-2018>, 2018.
- Liu, X., Rao, Z., Shen, C. C., Liu, J., Chen, J., Chen, S., Wang, X., and Chen, F.: Holocene Solar Activity Imprint on Centennial- to Multidecadal-Scale Hydroclimatic Oscillations in Arid Central Asia, *J. Geophys. Res.-Atmos.*, 124, 2562–2573, <https://doi.org/10.1029/2018JD029699>, 2019.
- Logan, A. J.: A new paleoclimate record for North Westland, New Zealand, with implications for the interpretation of speleothem based paleoclimate proxies, Master of Science, Geology, University of Canterbury, 109 pp., available at: <http://hdl.handle.net/10092/5762> (last access: 31 January 2020), 2011.
- Lončar, N., Bar-Matthews, M., Ayalon, A., Faivre, S., and Surić, M.: Holocene climatic conditions in the eastern Adriatic recorded in stalagmites from Strašna peć Cave (Croatia), *Quatern. Int.*, 508, 98–106, <https://doi.org/10.1016/j.quaint.2018.11.006>, 2019.
- Lorrey, A., Williams, P., Salinger, J., Martin, T., Palmer, J., Fowler, A., Zhao, J.-x., and Neil, H.: Speleothem stable isotope records interpreted within a multi-proxy framework and implications for New Zealand palaeoclimate reconstruction, *Quatern. Int.*, 187, 52–75, <https://doi.org/10.1016/j.quaint.2007.09.039>, 2008.
- Lorrey, A. M., Vandergoes, M., Renwick, J., Newnham, R., Acklerley, D., Bostock, H., Williams, P. W., King, D. N. T., Neil, H., Harper, S., et al.: A Regional Climate Regime Classification Synthesis for New Zealand Covering Three Critical Periods of the Late Quaternary: The Last 2000 Years, the Mid-Holocene, and the End of the Last Glacial Coldest Period; NIWA Client Report AKL2010-025; National Institute of Water and Atmospheric Research Ltd., Auckland, New Zealand, 2010.
- Marsh, A., Fleitmann, D., Al-Manmi, D. A. M., Altaweel, M., Wengrow, D., and Carter, R.: Mid- to late-Holocene archaeology, environment and climate in the north-east Kurdistan region of Iraq, *Holocene*, 28, 955–967, <https://doi.org/10.1177/0959683617752843>, 2018.
- McCabe-Glynn, S., Johnson, K. R., Strong, C., Berkelhammer, M., Sinha, A., Cheng, H., and Edwards, R. L.: Variable North Pacific influence on drought in southwestern North America since AD 854, *Nat. Geosci.*, 6, 617–621, <https://doi.org/10.1038/ngeo1862>, 2013.
- Medina-Elizalde, M., Burns, S. J., Polanco-Martinez, J. M., Beach, T., Lases-Hernandez, F., Shen, C. C., and Wang, H. C.: High-resolution speleothem record of precipitation from the Yucatan Peninsula spanning the Maya Preclassic Period, *Global Planet. Change*, 138, 93–102, <https://doi.org/10.1016/j.gloplacha.2015.10.003>, 2016.
- Medina-Elizalde, M., Burns, S. J., Polanco-Martinez, J., Lases-Hernandez, F., Bradley, R., Wang, H. C., and Shen, C. C.: Synchronous precipitation reduction in the American Tropics associated with Heinrich 2, *Sci. Rep.*, 7, 11216, <https://doi.org/10.1038/s41598-017-11742-8>, 2017.
- Moseley, G. E., Spötl, C., Brandstätter, S., Erhardt, T., Luetscher, M., and Edwards, R. L.: NALPS19: sub-orbital-scale climate variability recorded in northern Alpine speleothems during the last glacial period, *Clim. Past*, 16, 29–50, <https://doi.org/10.5194/cp-16-29-2020>, 2020.
- Mudelsee, M., Fohlmeister, J., and Scholz, D.: Effects of dating errors on nonparametric trend analyses of speleothem time series, *Clim. Past*, 8, 1637–1648, <https://doi.org/10.5194/cp-8-1637-2012>, 2012.
- Niggemann, S., Mangini, A., Mudelsee, M., Richter, D. K., and Wurth, G.: Sub-Milankovitch climatic cycles in Holocene stalagmites from Sauerland, Germany, *Earth Planet. Sc. Lett.*, 216, 539–547, [https://doi.org/10.1016/S0012-821X\(03\)00513-2](https://doi.org/10.1016/S0012-821X(03)00513-2), 2003a.
- Niggemann, S., Mangini, A., Richter, D. K., and Wurth, G.: A paleoclimate record of the last 17,600 years in stalagmites from the B7 cave, Sauerland, Germany, *Quaternary Sci. Rev.*, 22, 555–567, [https://doi.org/10.1016/S0277-3791\(02\)00143-9](https://doi.org/10.1016/S0277-3791(02)00143-9), 2003b.
- Ossete, M. L., Martin-Chivelet, J., Rossi, C., Edwards, R. L., Egli, R., Munoz-Garcia, M. B., Wang, X. F., Pavon-Carrasco, F. J., and Heller, F.: The Blake geomagnetic excursion recorded in a radiometrically dated speleothem, *Earth Planet. Sc. Lett.*, 353, 173–181, <https://doi.org/10.1016/j.epsl.2012.07.041>, 2012.
- Oster, J. L., Warken, S. F., Sekhon, N., Arienzo, M., and Lachniet, M.: Speleothem Paleoclimatology for the Caribbean, Central America, and North America, *Quaternary*, 2, 5, <https://doi.org/10.3390/quat2010005>, 2019.
- Parnell, A.: Bchron: Radiocarbon dating, age-depth modelling, relative sea level rate estimation, and non-parametric phase modelling, R package version 4.3.0, 2018.
- Partin, J. W., Quinn, T. M., Shen, C. C., Okumura, Y., Cardenas, M. B., Siringan, F. P., Banner, J. L., Lin, K., Hu, H. M., and Taylor, F. W.: Gradual onset and recovery of the Younger Dryas abrupt climate event in the tropics, *Nat. Commun.*, 6, 8061–8061, <https://doi.org/10.1038/ncomms9061>, 2015.
- Pawlak, J., Błaszczyk, M., Hercman, H., and Matoušková, Š.: A continuous stable isotope record of last interglacial age from the Bulgarian Cave Orlova Chuka, *Geochronometria*, 46, 87–101, <https://doi.org/10.1515/geochr-2015-0107>, 2019.
- Peckover, E. N., Andrews, J. E., Leeder, M. R., Rowe, P. J., Marca, A., Sahy, D., Noble, S., and Gawthorpe, R.: Coupled stalagmite – Alluvial fan response to the 8.2 ka event and early Holocene palaeoclimate change in Greece, *Palaeogeogr. Palaeoclimatol.*, 532, 109252–109252, <https://doi.org/10.1016/j.palaeo.2019.109252>, 2019.
- Polyak, V. J., Asmerom, Y., and Lachniet, M. S.: Rapid speleothem $\delta^{13}\text{C}$ change in southwestern North America coincident with Greenland stadial 20 and the Toba (Indonesia) supereruption, *Geology*, 45, 843–846, <https://doi.org/10.1130/g39149.1>, 2017.
- R Core Team: R: A language and environment for statistical computing, R Foundation for Statistical Computing, Vienna, Austria, available at: <http://www.r-project.org/index.html> (last access: 31 January 2020), 2019.

- Rehfeld, K. and Kurths, J.: Similarity estimators for irregular and age-uncertain time series, *Clim. Past*, 10, 107–122, <https://doi.org/10.5194/cp-10-107-2014>, 2014.
- Rehfeld, K., Goswami B., Juncu, D. Marwan N., and Breitenbach, S.: COPRA – Constructing Proxy Records From Age Models, Version 1.15, last mod. 2 November 2017, available at: <https://tocsy.pik-potsdam.de/copra.php> (last access: 31 January 2020), 2017.
- Rehfeld, K., Roesch, C., Comas-Bru, L., and Amirnezhad-Mozhdehi, S.: Age-depth model ensembles for SISAL v2 speleothem records (Version 1.0), Data set, Zenodo, <https://doi.org/10.5281/zenodo.3816804>, 2020.
- Rivera-Collazo, I., Winter, A., Scholz, D., Mangini, A., Miller, T., Kushnir, Y., and Black, D.: Human adaptation strategies to abrupt climate change in Puerto Rico ca. 3.5 ka, *Holocene*, 25, 627–640, <https://doi.org/10.1177/0959683614565951>, 2015.
- Roesch, C. and Rehfeld, K.: Automatising construction and evaluation of age-depth models for hundreds of speleothems, 9th International Workshop on Climate Informatics, Paris, France, 2–4 October, 2019.
- Rossi, C., Mertz-Kraus, R., and Osete, M. L.: Paleoclimate variability during the Blake geomagnetic excursion (MIS 5d) deduced from a speleothem record, *Quaternary Sci. Rev.*, 102, 166–180, <https://doi.org/10.1016/j.quascirev.2014.08.007>, 2014.
- Rossi, C., Bajo, P., Lozano, R. P., and Hellstrom, J.: Younger Dryas to Early Holocene paleoclimate in Cantabria (N Spain): Constraints from speleothem Mg, annual fluorescence banding and stable isotope records, *Quaternary Sci. Rev.*, 192, 71–85, <https://doi.org/10.1016/j.quascirev.2018.05.025>, 2018.
- Rudzka, D., McDermott, F., and Suric, M.: A late Holocene climate record in stalagmites from Modric Cave (Croatia), *J. Quaternary Sci.*, 27, 585–596, <https://doi.org/10.1002/jqs.2550>, 2012.
- Rudzka-Phillips, D., McDermott, F., Jackson, A., and Fleitmann, D.: Inverse modelling of the C-14 bomb pulse in stalagmites to constrain the dynamics of soil carbon cycling at selected European cave sites, *Geochim. Cosmochim. Ac.*, 112, 32–51, <https://doi.org/10.1016/j.gca.2013.02.032>, 2013.
- Scholz, D. and Hoffmann, D. L.: StalAge – An algorithm designed for construction of speleothem age models, *Quat. Geochronol.*, 6, 369–382, <https://doi.org/10.1016/j.quageo.2011.02.002>, 2011.
- Scroxton, N., Burns, S. J., McGee, D., Hardt, B., Godfrey, L. R., Ranivoharimanana, L., and Faina, P.: Competing Temperature and Atmospheric Circulation Effects on Southwest Madagascan Rainfall During the Last Deglaciation, *Paleoceanogr. Paleocl.*, 34, 275–286, <https://doi.org/10.1029/2018PA003466>, 2019.
- Sinha, N., Gandhi, N., Chakraborty, S., Krishnan, R., Yadava, M. G., and Ramesh, R.: Abrupt climate change at ~2800 yr BP evidenced by a stalagmite record from peninsular India, *Holocene*, 28, 1720–1730, <https://doi.org/10.1177/0959683618788647>, 2018.
- Staubwasser, M., Drăgușin, V., Onac, B. P., Assonov, S., Ersek, V., Hoffmann, D. L., and Veres, D.: Impact of climate change on the transition of Neanderthals to modern humans in Europe, *P. Natl. Acad. Sci. USA*, 115, 9116–9121, <https://doi.org/10.1073/pnas.1808647115>, 2018.
- Steponaitis, E., Andrews, A., McGee, D., Quade, J., Hsieh, Y. T., Broecker, W. S., Shuman, B. N., Burns, S. J., and Cheng, H.: Mid-Holocene drying of the US Great Basin recorded in Nevada speleothems, *Quaternary Sci. Rev.*, 127, 174–185, <https://doi.org/10.1016/j.quascirev.2015.04.011>, 2015.
- Strikis, N. M., Chiessi, C. M., Cruz, F. W., Vuille, M., Cheng, H., Barreto, E. A. D., Mollenhauer, G., Kasten, S., Karmann, I., Edwards, R. L., Bernal, J. P., and Sales, H. D.: Timing and structure of Mega-SACZ events during Heinrich Stadial 1, *Geophys. Res. Lett.*, 42, 5477–5484, <https://doi.org/10.1002/2015gl064048>, 2015.
- Strikis, N. M., Cruz, F. W., Barreto, E. A. S., Naughton, F., Vuille, M., Cheng, H., Voelker, A. H. L., Zhang, H., Karmann, I., Edwards, R. L., Auler, A. S., Santos, R. V., and Sales, H. R.: South American monsoon response to iceberg discharge in the North Atlantic, *P. Natl. Acad. Sci. USA*, 115, 3788–3793, <https://doi.org/10.1073/pnas.1717784115>, 2018.
- Talma, A. S. and Vogel, J. C.: Late Quaternary Paleotemperatures Derived from a Speleothem from Cango Caves, Cape Province, South Africa, *Quaternary Res.*, 37, 203–213, [https://doi.org/10.1016/0033-5894\(92\)90082-t](https://doi.org/10.1016/0033-5894(92)90082-t), 1992.
- Tan, L., An, Z., Huh, C.-A., Cai, Y., Shen, C.-C., Shiao, L.-J., Yan, L., Cheng, H., and Edwards, R. L.: Cyclic precipitation variation on the western Loess Plateau of China during the past four centuries, *Sci. Rep.*, 4, 6381–6381, <https://doi.org/10.1038/srep06381>, 2015.
- Tan, L., Cai, Y., Cheng, H., Edwards, L. R., Gao, Y., Xu, H., Zhang, H., and An, Z.: Centennial- to decadal-scale monsoon precipitation variations in the upper Hanjiang River region, China over the past 6650 years, *Earth Planet. Sc. Lett.*, 482, 580–590, <https://doi.org/10.1016/j.epsl.2017.11.044>, 2018a.
- Tan, L., Cai, Y., Cheng, H., Edwards, L. R., Lan, J., Zhang, H., Li, D., Ma, L., Zhao, P., and Gao, Y.: High resolution monsoon precipitation changes on southeastern Tibetan Plateau over the past 2300 years, *Quaternary Sci. Rev.*, 195, 122–132, <https://doi.org/10.1016/J.QUASCIREV.2018.07.021>, 2018b.
- Tzedakis, P. C., Drysdale, R. N., Margari, V., Skinner, L. C., Meniel, L., Rhodes, R. H., Taschetto, A. S., Hodell, D. A., Crowhurst, S. J., Hellstrom, J. C., Fallick, A. E., Grimalt, J. O., McManus, J. F., Martrat, B., Mokeddem, Z., Parrenin, F., Regattieri, E., Roe, K., and Zanchetta, G.: Enhanced climate instability in the North Atlantic and southern Europe during the Last Interglacial, *Nat. Commun.*, 9, 4235–4235, <https://doi.org/10.1038/s41467-018-06683-3>, 2018.
- van Breukelen, M. R., Vonhof, H. B., Hellstrom, J. C., Wester, W. C. G., and Kroon, D.: Fossil dripwater in stalagmites reveals Holocene temperature and rainfall variation in Amazonia, *Earth Planet. Sc. Lett.*, 275, 54–60, <https://doi.org/10.1016/J.EPSL.2008.07.060>, 2008.
- Van Rampelbergh, M., Fleitmann, D., Verheyden, S., Cheng, H., Edwards, L., De Geest, P., De Vleeschouwer, D., Burns, S. J., Matter, A., Claeys, P., and Keppens, E.: Mid- to late Holocene Indian Ocean Monsoon variability recorded in four speleothems from Socotra Island, Yemen, *Quaternary Sci. Rev.*, 65, 129–142, <https://doi.org/10.1016/j.quascirev.2013.01.016>, 2013.
- Verheyden, S., Keppens, E., Fairchild, I. J., McDermott, F., and Weis, D.: Mg, Sr and Sr isotope geochemistry of a Belgian Holocene speleothem: implications for paleoclimate reconstructions, *Chem. Geol.*, 169, 131–144, [https://doi.org/10.1016/s0009-2541\(00\)00299-0](https://doi.org/10.1016/s0009-2541(00)00299-0), 2000.
- Verheyden, S., Keppens, E., Quinif, Y., Cheng, H. J., and Edwards, L. R.: Late-glacial and Holocene climate reconstruc-

- tion as inferred from a stalagmite-Grotte du Père Noël, Han-sur-Lesse, Belgium, *Geol. Belg.*, 17, 83–89, available at: <https://popups.uliege.be/443/1374-8505/index.php?id=4412> (last access: 31 January 2020), 2014.
- Wang, J. K., Johnson, K. R., Borsato, A., Amaya, D. J., Griffiths, M. L., Henderson, G. M., Frisia, S., and Mason, A.: Hydroclimatic variability in Southeast Asia over the past two millennia, *Earth Planet. Sc. Lett.*, 525, 115737–115737, <https://doi.org/10.1016/j.epsl.2019.115737>, 2019.
- Wang, Y. J., Cheng, H., Edwards, R. L., Kong, X. G., Shao, X. H., Chen, S. T., Wu, J. Y., Jiang, X. Y., Wang, X. F., and An, Z. S.: Millennial- and orbital-scale changes in the East Asian monsoon over the past 224,000 years, *Nature*, 451, 1090–1093, <https://doi.org/10.1038/nature06692>, 2008.
- Ward, B. M., Wong, C. I., Novello, V. F., McGee, D., Santos, R. V., Silva, L. C. R., Cruz, F. W., Wang, X., Edwards, R. L., and Cheng, H.: Reconstruction of Holocene coupling between the South American Monsoon System and local moisture variability from speleothem $\delta^{18}\text{O}$ and $^{87}\text{Sr}/^{86}\text{Sr}$ records, *Quaternary Sci. Rev.*, 210, 51–63, <https://doi.org/10.1016/J.QUASCIREV.2019.02.019>, 2019.
- Warken, S. F., Fohlmeister, J., Schröder-Ritzrau, A., Constantin, S., Spötl, C., Gerdes, A., Esper, J., Frank, N., Arps, J., Terente, M., Riechelmann, D. F. C., Mangini, A. and Scholz, D.: Reconstruction of late Holocene autumn/winter precipitation variability in SW Romania from a high-resolution speleothem trace element record, *Earth Planet. Sc. Lett.*, 499, 122–133, <https://doi.org/10.1016/j.epsl.2018.07.027>, 2018.
- Warken, S. F., Scholz, D., Spötl, C., Jochum, K. P., Pajón, J. M., Bahr, A., and Mangini, A.: Caribbean hydroclimate and vegetation history across the last glacial period, *Quaternary Sci. Rev.*, 218, 75–90, <https://doi.org/10.1016/J.QUASCIREV.2019.06.019>, 2019.
- Webb, M., Dredge, J., Barker, P. A., Muller, W., Jex, C., Desmarchelier, J., Hellstrom, J., and Wynn, P. M.: Quaternary climatic instability in south-east Australia from a multiproxy speleothem record, *J. Quaternary Sci.*, 29, 589–596, <https://doi.org/10.1002/jqs.2734>, 2014.
- Weber, M., Scholz, D., Schröder-Ritzrau, A., Deininger, M., Spötl, C., Lugli, F., Mertz-Kraus, R., Jochum, K. P., Fohlmeister, J., Stumpf, C. F., and Riechelmann, D. F. C.: Evidence of warm and humid interstadials in central Europe during early MIS 3 revealed by a multi-proxy speleothem record, *Quaternary Sci. Rev.*, 200, 276–286, <https://doi.org/10.1016/J.QUASCIREV.2018.09.045>, 2018.
- Wendt, K. A., Häuselmann, A. D., Fleitmann, D., Berry, A. E., Wang, X., Auler, A. S., Cheng, H., and Edwards, R. L.: Three-phased Heinrich Stadial 4 recorded in NE Brazil stalagmites, *Earth Planet. Sc. Lett.*, 510, 94–102, <https://doi.org/10.1016/J.EPSL.2018.12.025>, 2019.
- Whittaker, T. E.: High-resolution speleothem-based palaeoclimate records from New Zealand reveal robust teleconnection to North Atlantic during MIS 1–4, unpublished PhD Thesis, The University of Waikato, 2008.
- Wilcox, P. S., Dorale, J. A., Baichtal, J. F., Spötl, C., Fowell, S. J., Edwards, R. L., and Kovarik, J. L.: Millennial-scale glacial climate variability in Southeastern Alaska follows Dansgaard-Oeschger cyclicity, *Sci. Rep.*, 9, 7880–7880, <https://doi.org/10.1038/s41598-019-44231-1>, 2019.
- Williams, P. W., King, D. N. T., Zhao, J. X., and Collerson, K. D.: Late pleistocene to holocene composite speleothem O-18 and C-13 chronologies from south island, new Zealand-did a global younger dryas really exist?, *Earth Planet. Sc. Lett.*, 230, 301–317, <https://doi.org/10.1016/j.epsl.2004.10.024>, 2005.
- Williams, P. W., Neil, H. L., and Zhao, J. X.: Age frequency distribution and revised stable isotope curves for New Zealand speleothems: palaeoclimatic implications, *Int. J. Speleol.*, 39, 99–112, <https://doi.org/10.5038/1827-806x.39.2.5>, 2010.
- Wu, J. Y., Wang, Y. J., Cheng, H., Kong, X. G., and Liu, D. B.: Stable isotope and trace element investigation of two contemporaneous annually-laminated stalagmites from northeastern China surrounding the “8.2 ka event”, *Clim. Past*, 8, 1497–1507, <https://doi.org/10.5194/cp-8-1497-2012>, 2012.
- Yadava, M. G., Ramesh, R., and Pant, G. B.: Past monsoon rainfall variations in peninsular India recorded in a 331-year-old speleothem, *Holocene*, 14, 517–524, <https://doi.org/10.1191/0959683604hl728rp>, 2004.
- Yin, J. J., Li, H. C., Rao, Z. G., Shen, C. C., Mii, H. S., Pillutla, R. K., Hu, H. M., Li, Y. X., and Feng, X. H.: Variations of monsoonal rain and vegetation during the past millennium in Tianguai Mountain, North China reflected by stalagmite delta O-18 and delta C-13 records from Zhenzhu Cave, *Quatern. Int.*, 447, 89–101, <https://doi.org/10.1016/j.quaint.2017.06.039>, 2017.
- Zhang, H., Cheng, H., Cai, Y., Spötl, C., Kathayat, G., Sinha, A., Edwards, R. L., and Tan, L.: Hydroclimatic variations in southeastern China during the 4.2 ka event reflected by stalagmite records, *Clim. Past*, 14, 1805–1817, <https://doi.org/10.5194/cp-14-1805-2018>, 2018a.
- Zhang, H., Cheng, H., Spötl, C., Cai, Y., Sinha, A., Tan, L., Yi, L., Yan, H., Kathayat, G., Ning, Y., Li, X., Zhang, F., Zhao, J., and Edwards, R. L.: A 200-year annually laminated stalagmite record of precipitation seasonality in southeastern China and its linkages to ENSO and PDO, *Sci. Rep.*, 8, 12344–12344, <https://doi.org/10.1038/s41598-018-30112-6>, 2018b.
- Zhang, H., Ait Brahim, Y., Li, H., Zhao, J., Kathayat, G., Tian, Y., Baker, J., Wang, J., Zhang, F., Ning, Y., Edwards, L. R., and Cheng, H.: The Asian Monsoon: Teleconnections and Forcing Mechanisms – A Review from Chinese Speleothem $\delta^{18}\text{O}$ Records, *Quaternary*, 2, 26, <https://doi.org/10.3390/quat2030026>, 2019.
- Zhang, H. B., Griffiths, M. L., Huang, J. H., Cai, Y. J., Wang, C. F., Zhang, F., Cheng, H., Ning, Y. F., Hu, C. Y., and Xie, S. C.: Antarctic link with East Asian summer monsoon variability during the Heinrich Stadial-Bølling interstadial transition, *Earth Planet. Sc. Lett.*, 453, 243–251, <https://doi.org/10.1016/j.epsl.2016.08.008>, 2016.
- Zhang, H. L., Yu, K. F., Zhao, J. X., Feng, Y. X., Lin, Y. S., Zhou, W., and Liu, G. H.: East Asian Summer Monsoon variations in the past 12.5 ka: High-resolution $\delta^{18}\text{O}$ record from a precisely dated aragonite stalagmite in central China, *J. Asian Earth Sci.*, 73, 162–175, <https://doi.org/10.1016/j.jseaes.2013.04.015>, 2013.
- Zhang, P., Cheng, H., Edwards, R. L., Chen, F., Wang, Y., Yang, X., Liu, J., Tan, M., Wang, X., Liu, J., An, C., Dai, Z., Zhou, J., Zhang, D., Jia, J., Jin, L., and Johnson, K. R.: A Test of Climate, Sun, and Culture Relationships from

an 1810-Year Chinese Cave Record, *Science*, 322, 940–942,
<https://doi.org/10.1126/science.1163965>, 2008.